ISSN 2355-3286

ULTIMA Computing

Jurnal Sistem Komputer

Engineering | Vol. 14 | No. 2 | Page 48 - 87 | December 2022 | ISSN 2355-3286

UMN

UNIVERSITAS
MULTIMEDIA
NUSANTARA

ISSN 2355-3286

EDITORIAL BOARD

EDITORIAL ADDRESS

Universitas Multimedia Nusantara (UMN)
Jl. Scientia Boulevard
Gading Serpong
Tangerang, Banten - 15811
Indonesia
Phone. (021) 5422 0808
Fax. (021) 5422 0800
Email : ultimacomputing@umn.ac.id

Ultima Computing : Jurnal Sistem Komputer is a Journal of Computer Engineering Study Program, Universitas Multimedia Nusantara which presents scientific research articles in the field of Computer Engineering and Electrical Engineering as well as current theoretical and practical issues, including Edge Computing, Internet-of-Things, Embedded Systems, Robotics, Control System, Network and Communication, System Integration, as well as other topics in the field of Computer Engineering and Electrical Engineering. The Ultima Computing : Jurnal Sistem Komputer is published regularly twice a year (June and December) and is jointly managed by the Computer Engineering and Electrical Engineering Study Program at Universitas Multimedia Nusantara.

Call for Papers

International Journal of New Media Technology (IJNMT) is a scholarly open access, peer-reviewed, and interdisciplinary journal focusing on theories, methods and implementations of new media technology. Topics include, but not limited to digital technology for creative industry, infrastructure technology, computing communication and networking, signal and image processing, intelligent system, control and embedded system, mobile and web based system, and robotics. IJNMT is published twice a year by Faculty of Engineering and Informatics of Universitas Multimedia Nusantara in cooperation with UMN Press.

Ultimatics : Jurnal Teknik Informatika is the Journal of the Informatics Study Program at Universitas Multimedia Nusantara which presents scientific research articles in the fields of Analysis and Design of Algorithm, Software Engineering, System and Network security, as well as the latest theoretical and practical issues, including Ubiquitous and Mobile Computing, Artificial Intelligence and Machine Learning, Algorithm Theory, World Wide Web, Cryptography, as well as other topics in the field of Informatics.

Ultima Computing : Jurnal Sistem Komputer is a Journal of Computer Engineering Study Program, Universitas Multimedia Nusantara which presents scientific research articles in the field of Computer Engineering and Electrical Engineering as well as current theoretical and practical issues, including Edge Computing, Internet-of-Things, Embedded Systems, Robotics, Control System, Network and Communication, System Integration, as well as other topics in the field of Computer Engineering and Electrical Engineering.

Ultima InfoSys : Jurnal Ilmu Sistem Informasi is a Journal of Information Systems Study Program at Universitas Multimedia Nusantara which presents scientific research articles in the field of Information Systems, as well as the latest theoretical and practical issues, including database systems, management information systems, system analysis and development, system project management information, programming, mobile information system, and other topics related to Information Systems.

ISSN 2355-3286

FOREWORD

ULTIMA Greetings!

Ultima Computing : Jurnal Sistem Komputer is a Journal of Computer Engineering and Electrical Engineering at Multimedia Nusantara University which presents scientific research articles in the field of Computer Systems as well as the latest theoretical and practical issues, including Edge Computing, Internet-of-Things, Embedded Systems, Robotics, Control Systems, Network and Communication, System Integration, and other topics in the field of Computer Engineering and Electrical Engineering.

In this December 2022 edition, ULTIMA Computing enters the 2nd Edition of Volume 14. In this edition there are six scientific papers from researchers, academics and practitioners in the fields of Computer Engineering and Electrical Engineering. Some of the topics raised in this journal are: Black Hole Detection Using Modified Sequence Number in Vehicular Ad-hoc Network, Water Flow & Temperature Control to Increase Extraction Yield of Light-roasted Coffee Beans, Light Emiting Diode Control System based on the Microcontroller and Smartphone Application, Semi-Automatic Medical Syringe Pump Development: Interface, Control, Alarm, and Feedback, Dynamic Ultrasonic Wave Generators as an Alternative Technology to Field Rat Repellents and An Analysis Of The Performance Of Autonomous Navigation On An Ardupilot-Controlled Rover.

On this occasion we would also like to invite the participation of our dear readers, researchers, academics, and practitioners, in the field of Engineering and Informatics, to submit quality scientific papers to: International Journal of New Media Technology (IJNMT), Ultimatics : Jurnal Teknik Informatics, Ultima Infosys: Journal of Information Systems and Ultima Computing: Journal of Computer Systems. Information regarding writing guidelines and templates, as well as other related information can be obtained through the email address ultimacomputing@umn.ac.id and the web page of our Journal here.

Finally, we would like to thank all contributors to this December 2022 Edition of Ultima Computing. We hope that scientific articles from research in this journal can be useful and contribute to the development of research and science in Indonesia.

December 2022,

M.B.Nugraha, S.T., M.T.
Editor-in-Chief

ISSN 2355-3286

TABLE OF CONTENT

ISSN 2355-3286

Black Hole Detection Using Modified Sequence Number in Vehicular Ad-hoc Network

Rakha Fikran Julda[1], Dany Primanita Kartikasari[2], Rakhmadhany Primananda[3]
[1,2,3] Informatics Engineering, Brawijaya University, Malang, Indonesia
[1]rakhafikran@gmail.com, [2]dany.jalin@ub.ac.id, [3]rakhmadhany@ub.ac.id

Accepted 08 September 2022
Approved 20 October 2022

***Abstract*— Vehicular Ad-hoc Network (VANET) is a type of wireless network with Dedicated Short-Range Communication (DSRC) that enables communication between vehicles (V2V) and communication between vehicles to infrastructure around them (V2I). VANET has several security requirements to consider in order to maintain the network functionality. Availability is the most important security requirement due to its responsibility of maintaining the functionality of the network, attack on availability may cause the lack of availability and reduce the efficiency of VANET. One of the attack that threat the availability of VANET is black hole. In this paper, we address the problem of black hole attack in VANET, using Modified Sequence Number (MSN) as a detection method. The simulation is performed using NS-2 as a simulator and AODV as a routing protocol. Detection Rate (DR) and False Alarm Rate (FAR) are used to evaluate the performance of MSN algorithm in detecting black hole attack. Evaluation with variation in the number of CBR packets shows that MSN algorithm successfully detects black hole attacks with DR values reaching 69.0909% at 10 CBR packets and FAR values reaching 0.0037 at 20 CBR packets. We also evaluate the performance of MSN algorithm with variations of node density. The evaluation shows that MSN algorithm successfully detects black hole attack with DR values reaching 100% with a density of 10 and 20 nodes, with the percentage of FAR values reaching 0% in all numbers of node density.**

***Index Terms*— AODV; Black Hole Attacks; VANET**

I. INTRODUCTION

VANET is a dedicated short-range communication (DSRC) wireless network technology that works on the 5.9 GHz frequency spectrum for communication between vehicles. Unlike MANET which uses IEEE 802.11a/g/n, the physical layer of VANET uses the IEEE 802.11p standard protocol with its focus on communication in Intelligent Transportation Systems (ITS) environment [1]. In VANET, there are two types of communication that take place. Vehicle-to-Vehicle (V2V) is a communication between vehicles, whereas Vehicle-to-Infrastructure (V2I) communication is between vehicles and infrastructure such as Roadside Units. (RSU) [2]. VANET has several parameter to ensure its network security, including integrity, authentication, availability, privacy, and non-repudiation. Attackers exploit these security parameter to carry out their attack. The primary role of availability to guarantee the network services continue to work in the event of malicious attacks is what makes availability one of the most important parameter in VANET security, as its lack of availability may diminish the efficiency of VANET [3]. One of the attack that threat the availability of VANET is black hole [4]. Black hole use the routing protocol's route discovery process which searches for the nearest route, by pretending to be the node with the newest and shortest path to destination. The black hole node that receives the packet drops the packet so that the packet is not received by the destination. The routing table of the routing protocol is disrupted by the behavior of black hole attacks, reducing the performance efficiency of VANET [5]. Therefore, a routing protocol that can works on network with dynamic topologies, high mobility, and able to protect against attacks such as black hole is required.

In attempt to secure VANET from black hole attack, several research has been done. Among these is using a protocol called Secure AODV (SAODV). The proposed routing protocol changes the destination IP address of AODV packet request by applying Cyclic Redundancy Check 32 bits (CRC-32) as a hash function, resulting a secure AODV RREQ packet without any extra overhead. The test results in this study explain that the proposed protocol successfully addresses black hole attack with PDR performance, end-to-end delay, routing overhead, and throughput that is nearly identical to traditional AODV. Additionally, the proposed protocol has a high detection rate at both high and low node density [6]. However, the research has not shown the performance of SAODV in dealing with black hole attack with variation in number of packets sent. The variation in number of packets sent can determine how well a method to detect black hole attack [7]. Therefore, we use a scenario with different number of Constant Bit Rate (CBR) packet sent to measure the performance of our propose method.

Another research to secure wireless network from black hole attack is by implementing Modified Sequence Number (MSN) in MANET by using Route Reply (RREP) Sequence Number (SN) as the threshold. The threshold is set based on the highest SN value that the source can accept. When the source receive an RREP packet with a SN value above the threshold, the source will rebroadcast RREQ packet using RREP SN as the source SN. When the source receives a RREP message from the same node and the SN value of the RREP still exceeds the specified threshold, it will detect the route with the black hole node and is not used to forward the data. The research shows that the proposed method has higher PDR and throughput values in dealing with black hole at both low and high node densities compare to normal AODV and IDS [8]. The research, however, has not shown how well MSN in detecting black hole attack in AODV. Therefore, we use detection rate as a parameter to evaluate our propose method in detecting black hole attack.

According to prior research that assessed the performance of AODV on VANET, the fall in packet delivery ratio (PDR) on the performance of AODV in black hole attack reached 60% [6]. Therefore, a method that capable of protecting VANET from black hole attack is needed. In this paper, we propose a method to detect black hole attack in VANET by implementing MSN with AODV routing protocol. The performance of MSN algorithm in detecting black hole attack is tested based on variations in the number of Constant Bit Rate (CBR) packets and node density using Network Simulator 2 (NS-2).

II. Literature Review

A. *Vehicular Ad-hoc Network*

Vehicular Ad-hoc Network (VANET) Vehicular Ad Hoc Network (VANET) is a development of Mobile Ad Hoc Network (MANET) technology that allows vehicles to communicate with one another and share information about road conditions, as well as share various types of warnings [9]. VANET communication is based on IEEE standard known as Wireless in Vehicular Environment (WAVE). WAVE is the result of the development of 802.11, specifically 802.11p, which allocate 75 MHz bandwidth in the 5.9 GHz frequency spectrum for V2V and V2I communication. At 5.9 GHz, the 75 MHz spectrum is split into 7 channels, each with a 10 MHz bandwidth. Figure 1 depicts the 5.9 GHz frequency spectrum's channel segmentation. [2].

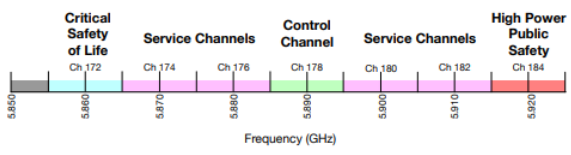

Fig. 1. Channels bandwidth allocation at 5.9 GHz frequency spectrum

In VANET, vehicles communicate with each other to share information needed for safety, comfort, and entertainment. The VANET communication architecture is divided into four categories [10]:

- In-vehicle communication: It is communication that aims to detect the condition of the vehicle and the driver
- Vehicle-to-vehicle: Communication between vehicles that is useful for sharing various kinds of information such as route information, various warnings, and information between drivers.
- Vehicle-to-infrastructure: It is communication that occurs between vehicles and the surrounding infrastructure such as the Road Side Unit (RSU). RSU on functions like a router that receives and sends information received from the vehicle and sends it to the intended destination. RSUs are allocated on the roadside with coverage distances depending on the equipment used.
- Vehicle-to-broadband communication: This means that communication on VANET vehicles can connect to other wireless network channels such as 3G and 4G because the cloud from the broadband can receive traffic information and monitoring data that can be useful for tracking vehicle location.

The VANET architecture is made up of vehicle-to-vehicle (V2V) and vehicle-to-infrastructure (V2I) connectivity (V2I). The VANET system's supporting components are divided into two parts [11]:

- On-board Unit (OBU): OBU is a device in the vehicle to provide both V2V and V2I communication that placed on the vehicles.
- Roadside Unit (RSU): A network device that provide connectivity to various OBUs to the internet.

In order to secure communication in VANET, there are several parameters that need to be consider. The parameters that ensure this security are as follows [3]:

- Authentication: Ensure that the data entered by the user is correctly entered by the validated user, and that the data entered by the receiver is correctly entered by the sender.
- Availability: This is an important security parameter for VANETs since it is directly linked to the availability of security applications. VANET management must ensure the availability of services in the event of a problem or a malfunction.
- Confidentiality: Ensure that the message sent by the sender may only be accessed by the receiver.
- Integrity: Ensuring that the message sent by the sender does not change when it is received by the receiver.

B. Ad-hoc On-Demand Distance Vector

Ad-hoc On-demand Distance Vector (AODV) is commonly used routing protocol and a part of reactive routing protocols that work on-demand, which means that the protocol only establishes the path when it receive request from the node to engage in communication [12]. The AODV protocol utilizes two different mechanisms: route discovery and route maintenance. In discovering the route AODV broadcast a route request (RREQ) message to the neighboring node until it receives by the destination node. The destination or neighbor node that has a direct route to the destination receives RREQ, it will send a unicast route reply (RREP) message to the source node via a route where RREQ received (reverse route). The route to send the data will be chosen from the intermediate or destination node with a lowest hop count and a newest sequence number that is stored in the routing table. To notify if a route cannot be used, a Route Error message (RERR) is delivered and set the error route with invalid flag. If an invalid route is needed again, the route discovery process is repeated to find that route. The following are the fields stored on each AODV node [13]:

- Destination address: Contains the IP address of the destination node
- Sequence number: A number that continues to increase when an RREQ, RREP, and REER message is sent. The sequence number is used to determine the freshness of a route.
- Next hop: Store the address of the neighboring node.
- Hop count: The number of hops from the source node to the destination node.
- Lifetime: The time it takes for a node to receive the RREP message in milliseconds.

Routing flags: Showing the status of a route that shows valid if the route can still be used and shows invalid for routes that cannot be used.

C. Black Hole Attacks

Black hole attack is an attack carried out by pretending to be the shortest route to the destination which aims to get data and drop packets without continuing the message to the destination [14]. The black hole attack process is carried out by utilizing the route discovery process. When the source node sends an RREQ message, the attacker node pretends to have the shortest and newest route to the destination node by sending RREP packet with the lowest hop count and highest sequence number to the source node. This causes the source node to ignore RREP messages from other intermediate nodes and choose the route with the attacker node on it. Attacker node will drop the data that get through it, causing the data to never reach the destination node [6].

Figure 2 depicts AODV route discovery phase under black hole attack. As shown in the figure, the attack begins with the source node (S) broadcasting an RREQ message to the entire network in order to transfer data to the destination node (D). D which receives an RREQ from S then sends a RREP message with a hop count value of 2 and a sequence number of 125 through node I. When node M, a black hole node, gets an RREQ message, M sends an RREP message with the altered hop count and sequence number values of 1 and 4294967295. Because the AODV routing protocol takes the shortest delivery route indicated by the least hop count value and the latest route indicated by the greatest sequence number value, S who receives both RREP from D and M will choose the M route, which is a route that has black hole node on it, as a data transmission path [15].

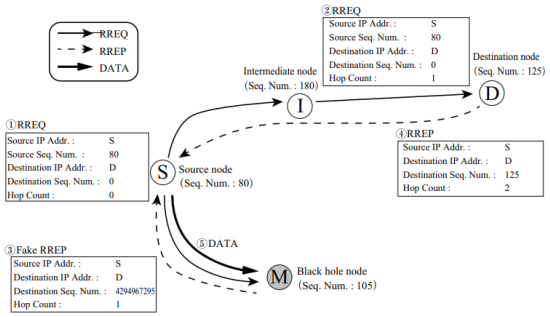

Fig. 2. Black hole attack in AODV

D. Modified Sequence Number

Modified Sequence Number (MSN) is a black hole attack detection method by utilizing the attack nature of the black hole that sends a RREP message with the highest sequence number (SN) value so that it is considered the latest path by the routing protocol. MSN detects black hole attack by establishing a threshold based on the maximum SN value of the RREP message that can be received by the source. If the RREP message received by the source has an SN value greater than the threshold, the source resends the RREQ message with the RREP sequence number as the retransmitted RREQ message's sequence number. When the source receives back an RREP message from the same node whose SN value is equal to the determined threshold value, the node is identified as a black hole attack, and the path from the message sent is not used to transmit data [8].

```
1   Src broadcast RREQ
2   Wait for RREP
3   On Receiving RREP
4   IF (RREP Sequence Number - SSN > TH)  {
5      RRq by changing SSN to RREPSN
6      Wait for RREP
7      IF (RREPSN - SSN > TH)  {
8      Black hole detected
9      Discard the route
10     }
11  }
12  Else {
13     Send data using the route
```

14	}

Fig. 3. Pseudocode of MSN algorithm

The following is an explanation of the notation of the pseudocode in Fig.3 :

- Src: Source Node
- RRq: Re-broadcast RREQ
- SSN: Source sequence number
- RREPSN: Route reply sequence number
- TH: threshold

III. METHODOLOGY

Figure 4 illustrates the design that is the basis for the implementation of this research. The implementation begins by modifying the aodv.h and aodv.cc files by adding black hole attacks and MSN as black hole detection method. After modifying those files, black hole attack and added detection method are used in simulations in NS-2. The results of the simulation are in the form of a trace file and then processed using an AWK script that produces test metrics, namely detection rate (DR) and false alarm rate (FAR).

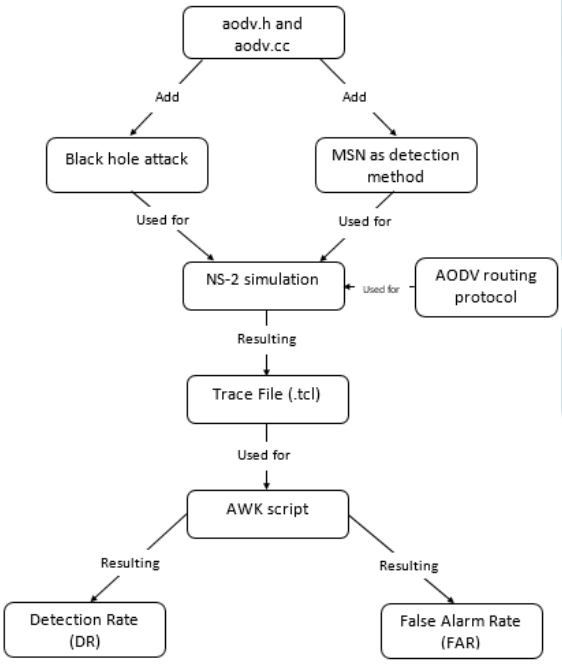

Fig. 4. Implementation Flow

To evaluate the performance of MSN algorithm, a sets of simulation were run on NS-2. The parameters of the simulations are detailed in Table 1.

TABLE I. SIMULATION PARAMETERS

Parameter	Value
Simulator	Network Simulator 2 (ns-2.35), SUMO
Routing Protocol	AODV
Network Area	1000 m x 800 m
Packet Type	CBR
MAC	802.11p
Number of Nodes	20, 40, 50, 60, 80, 100
Attack Type	Black hole
Number of Attacker Nodes	1
Simulation Time	200 second
Packet Size	512 Kb
Number of CBR Packets Send	1, 5, 10, 15, 20
Mobility Model	Random way point

In the simulations, we chose one of the node as a black hole node, we assume that black hole nodes respond all RREQs with forged destination sequence number. The forged sequence number is the real sequence number from RREQ + 100 which is used as threshold.

To measure the performance of MSN algorithm in detecting black hole we use two different scenarios, node density and variations in number of CBR packets sent. The node density test was performed to determine the success of the MSN algorithm in identifying black hole attacks on VANET with varying vehicle counts [16]. Simulation of node density testing is performed on NS-2 with a total of one CBR package, one black hole node, and density variations of 20, 40, 60, 80, and 100 nodes. The scenario testing of the number of CBR packets was performed on NS-2 with a node density of 50 nodes, one black hole node, and changes in the number of CBR packets transmitted of 1, 5, 10, 15, and 20.s

The evaluation of MSN algorithm performance was done based on two parameters, Detection Rate (DR) and False Alarm Rate (FAR). DR is a method to measure the successfulness of MSN algorithm in detecting black hole attack. Equation (1) can be used to calculate the DR, whereas the FAR is a function used to measure the percentage error of a method in detecting attacks. The equation (2) can be used to calculate the FAR [7].

$$DR = \frac{TP}{TP + FN} X\ 100\% \quad (1)$$

With:

TP: Attacker node classified as attack.
FN: Normal node classified as attack.

$$FAR = \frac{FP}{TN + FP} X\ 100\% \quad (2)$$

With:

FP: Attack node classified as normal.
TN: Normal node classified as normal.

IV. Results and Discussion

The first test to evaluate the detection performance of the MSN algorithm is to calculate the algorithm's DR value. Tests are run to determine the algorithm's success in detecting black hole attack on the network. The following are the findings of the MSN algorithm's DR testing against the two scenarios:

TABLE II. The results of DR tests on variations in the number of CBR packets

Number of CBR Packets Sent	True Positive (TP)	False Negative (FN)	Detection Rate (DR)%
1	38	17	69.0909
5	178	120	59.7315
10	457	321	58.7404
15	1188	1501	44.1800
20	2106	2738	43.4765

The results of the DR test on variations in the number of CBR packets with values of 1, 5, 10, 15, and 20 are shown in Table 2. The table of test results shows that the more CBR packets sent, the higher the TP and FN values, which influences the value of DR that determines the success of algorithm in detecting black hole attack. The results of the tests reveal that the MSN algorithm detection performance based on the DR parameter obtains the highest results in single CBR packet delivery, with the DR value reaching 69.0909% and dropping as the number of CBR packets grows, with the lowest value at 20 packets reaching 43.4765%.

TABLE III. The results of DR tests on variations in node density

Node Density	True Positive (TP)	False Negative (FN)	Detection Rate (DR)%
20	18	0	100
40	27	12	69.2038
60	17	10	62.9630
80	22	10	68.7500
100	30	0	100

Table 3 shows the results of the DR test on node density changes of 20, 40, 60, 80, and 100 nodes. The results shows that the MSN algorithm succeeded in detecting black hole attack at various node density situations, with DR values reaching 100% for densities of 20 and 100 nodes.

Another test to evaluate the performance of MSN algorithm is by testing it using FAR to calculate the detection error percentage in detecting black hole attack. The following are the results of the MSN algorithm's FAR testing against the two scenarios:

TABLE IV. The results of FAR tests on variations in the number of CBR packets.

Number of CBR Packets Sent	True Positive (TP)	False Negative (FN)	False Alarm Rate (FAR)%
1	0	37868	0.0000
5	0	141190	0.0000
10	0	341465	0.0000
15	2	721700	0.0003
20	47	1266549	0.0037

Table 4 shows the results of FAR testing on variations in the number of CBR packages with values of 1, 5, 10, 15, and 20. The results shows that the more CBR packages sent, the higher the TP and FN values, which influences the value of FAR. Table 5 shows that the MSN algorithm detection performance based on the FAR parameter is best when just one CBR packet is delivered at a time, and degrades as the number of CBR packets grows.

TABLE V. The results of DR tests on variations in node density.

Node Density	True Positive (TP)	False Negative (FN)	False Alarm Rate (FAR)%
20	0	9904	0,0000
40	0	22041	0,0000
60	0	30949	0,0000
80	0	47345	0,0000
100	0	67617	0,0000

Table 5 shows the results of the DR test on node density changes of 20, 40, 60, 80, and 100 nodes. The table of test results shows that the MSN algorithm detected black hole attacks in VANET at various node densities with a FAR value of 0.0000%.

V. Conclusion

To detect black hole attacks on VANET, this research implements the Modified Sequence Number (MSN) algorithm as a detection method. Based on results of the experiments, the MSN algorithm was successful in detecting black hole attacks on VANET. This success is shown by the detection rate (DR) test parameter value reaching 69.0909% when testing the number of CBR packets sent and 100% for testing the density of network nodes. The false alarm rate (FAR) test parameter is also used to determine the percentage of detection errors from the detection method. FAR testing results in the maximum percentage of detection errors, reaching 0.0037% when measuring the amount of CBR packets sent and 0% when testing network node density. From the research conducted, the success of the

MSN algorithm still does not take into account the effect of the characteristic parameters on the VANET on the DR and FAR test parameters, and does not take into account the detection method for the QoS of the VANET network. These two things can be the focus of further research.

REFERENCES

[1] A. Fitah, A. Badria, M. Moughit, and A. Sahel, "Performance of DSRC and WIFI for intelligent transport systems in VANET," *Procedia Comput. Sci.*, vol. 127, pp. 360–368, 2018, doi: 10.1016/j.procs.2018.01.133.

[2] F. Arena, G. Pau, and A. Severino, "A review on IEEE 802.11p for intelligent transportation systems," *J. Sens. Actuator Networks*, vol. 9, no. 2, pp. 1–11, 2020, doi: 10.3390/jsan9020022.

[3] J. Liang, M. S. Sheikh, and W. Wang, "A survey of security services, attacks, and applications for vehicular ad hoc networks (VANETs)," *Sensors (Switzerland)*, vol. 19, no. 16, 2019, doi: 10.3390/s19163589.

[4] Z. Afzal and M. Kumar, "Security of Vehicular Ad-Hoc Networks (VANET): A survey," *J. Phys. Conf. Ser.*, vol. 1427, no. 1, 2020, doi: 10.1088/1742-6596/1427/1/012015.

[5] J. Grimaldo, *Performance comparison of routing protocols in VANETs under black hole attack in Panama City; Performance comparison of routing protocols in VANETs under black hole attack in Panama City*. 2018. doi: 10.1109/CONIELECOMP.2018.8327187.

[6] S. Lachdhaf, M. Mazouzi, and M. Abid, "Detection and Prevention of Black Hole Attack in VANET Using Secured AODV Routing Protocol," pp. 25–36, 2017, doi: 10.5121/csit.2017.71503.

[7] H. Moudni, M. Er-Rouidi, H. Mouncif, and B. El Hadadi, "Black Hole attack Detection using Fuzzy based Intrusion Detection Systems in MANET," *Procedia Comput. Sci.*, vol. 151, pp. 1176–1181, 2019, doi: 10.1016/j.procs.2019.04.168.

[8] S. Shrestha, R. Baidya, B. Giri, and A. Thapa, "Securing Blackhole Attacks in MANETs using Modified Sequence Number in AODV Routing Protocol," *2020 8th Int. Electr. Eng. Congr. iEECON 2020*, pp. 2020–2023, 2020, doi: 10.1109/iEECON48109.2020.229555.

[9] H. F. Mahdi, M. S. Abood, and M. M. Hamdi, "Performance evaluation for vehicular ad-hoc networks based routing protocols," *Bull. Electr. Eng. Informatics*, vol. 10, no. 2, pp. 1080–1091, 2021, doi: 10.11591/EEI.V10I2.2943.

[10] T. Zaidi and S. Faisal, "An overview: Various attacks in VANET," *2018 4th Int. Conf. Comput. Commun. Autom. ICCCA 2018*, no. July, pp. 1–6, 2018, doi: 10.1109/CCAA.2018.8777538.

[11] H. Hasrouny, A. E. Samhat, C. Bassil, and A. Laouiti, "VANet security challenges and solutions: A survey," *Veh. Commun.*, vol. 7, no. January, pp. 7–20, 2017, doi: 10.1016/j.vehcom.2017.01.002.

[12] A. D. Devangavi and R. Gupta, "Routing protocols in VANET-A survey," *Proc. 2017 Int. Conf. Smart Technol. Smart Nation, SmartTechCon 2017*, pp. 163–167, May 2018, doi: 10.1109/SMARTTECHCON.2017.8358362.

[13] C. Perkins, E. Belding-Royer, and S. Das, "Network Working Group," 2003.

[14] S. Tanwar, J. Vora, S. Tyagi, N. Kumar, and M. S. Obaidat, "A systematic review on security issues in vehicular ad hoc network," *Secur. Priv.*, vol. 1, no. 5, p. e39, 2018, doi: 10.1002/spy2.39.

[15] T. Noguchi and M. Hayakawa, "Black Hole Attack Prevention Method Using Multiple RREPs in Mobile Ad Hoc Networks," *Proc. - 17th IEEE Int. Conf. Trust. Secur. Priv. Comput. Commun. 12th IEEE Int. Conf. Big Data Sci. Eng. Trust. 2018*, pp. 539–544, 2018, doi: 10.1109/TrustCom/BigDataSE.2018.00082.

[16] R. Khatoun, P. Gut, R. Doulami, L. Khoukhi, and A. Serhrouchni, "A reputation system for detection of black hole attack in vehicular networking," *2015 Int. Conf. Cyber Secur. Smart Cities, Ind. Control Syst. Commun. SSIC 2015 - Proc.*, no. August, 2015, doi: 10.1109/SSIC.2015.7245328.

ISSN 2355-3286

Water Flow & Temperature Control to Increase Extraction Yield of Light-roasted Coffee Beans

Samuel Hutagalung
Computer Engineering, Universitas Multimedia Nusantara, Tangerang, Indonesia
samuel.hutagalung@umn.ac.id

Accepted 04 October 2022
Approved 11 November 2022

***Abstract*— Using light-roasted coffee beans for brewing espresso poses a general problem for pump-based espresso machines. Soluble in light-roasted coffee beans is more challenging to extract and requires a higher EY percentage because it has a relatively higher acidity level than dark-roasted coffee beans. The extraction range of 18% - 22% in light-roasted coffee beans for espresso brewing with an 8% - 12% TDS is qualitatively considered insufficient to produce espresso with a balanced taste. To improve the extraction ability of the espresso machine on coffee soluble. We design two features that hypothetically can solve the problem: Temperature Control Module to increase water temperature stability as a replacement for the thermostat, and Flow Control Module to regulate the speed of the vibration pump by adjusting the voltage resistance to reduce the water pressure/ flow rate used during the initial extraction at the preinfusion phase. Based on the results of trials using an espresso machine that has added temperature and flow control modules, there is an increase in the average percentage of extraction compared to the results of trials using stock machines; the average extraction percentage increased by 4.83 points. Qualitatively, this increase of %EY also significantly impacts the espresso taste, which tasted very sour and unbalanced, became relatively more balanced and comfortable to enjoy.**

***Index Terms*— espresso machine; extraction yield percentage; flow control; light-roasted coffee; preinfusion.**

I. The Problem

Coffee drinks are made by extracting the soluble from coffee beans to be dissolved in water. Several factors influence water's ability to extract the solubility in coffee beans, such as [1][2][3][4][5]:

- Water temperature.
- The ratio of the amount of water to coffee beans.
- Duration of extraction.
- Agitation.
- The particle size of coffee beans.
- The solubility of coffee beans.

The solubility of coffee beans received particular attention in this study. Dark-roasted coffee beans have a higher solubility than light-roasted coffee beans. Water more easily extract the soluble in dark-roasted coffee beans than light-roasted coffee beans. [6][7]

Espresso is a coffee drink with 8% - 12% Total Dissolved Solids (TDS) and 18% - 22% Extraction Yield (EY). With the composition of TDS and EY in these ranges, the extraction process that needs to be carried out by an espresso machine will be relatively more challenging than 1.15% - 1.35% TDS pour-over coffee drinks. Therefore, in brewing espresso, cafe generally uses dark-roasted coffee beans because of their relatively easy characteristics to be extracted to 18% - 22% EY with only a little water in 8% - 12% TDS. [8]

On the other hand, the trend of using light-roasted coffee beans continues to increase along with the current development of the coffee industry (the third wave of coffee), where the quality of green beans from the harvests of farmers is relatively better and can be classified as specialty coffee (based on Specialty Coffee Association standard):

- No more than five full defects in 300 grams of coffee.
- No primary defects.
- A maximum of 5% is tolerated or below the screen size indicated.
- Free of faults and stains.
- No Quakers are permitted.
- Moisture content is between 9-13%.

However, using light-roasted coffee beans for brewing espresso poses a general problem for pump-based espresso machines. Soluble in light-roasted coffee beans is more challenging to extract and requires a higher EY percentage because it has a relatively higher acidity level than dark-roasted coffee beans [9]. The extraction range of 18% - 22% in light-roasted coffee beans for espresso brewing with an 8% - 12% TDS is qualitatively considered insufficient to produce espresso with a balanced taste.

To achieve a higher %EY for light-roasted coffee beans, the extraction process that needs to be carried out by an espresso machine is also no longer able to follow the standard SCA (Specialty Coffee Association) method, where the extraction duration is limited to 30 seconds and the pressure used is 9 bar from start to finish. We have conducted trials to prove the research problem to be solved, using a standard Delonghi ECP33.21 espresso machine with the traditional SCA method and a Mazzer Super Jolly grinder with a 33M burrs set. The coffee used in the trial was light-roasted arabica from Kenya and roasted by Space Roastery Jogja. Based on the trial results in Table 1, the maximum %EY that can be achieved was 18.97%, with an average of 18.59% from 12 trials (the maximum number that the related machine can make in 1 water tank filling). In these conditions, with light-roasted coffee beans, the espresso taste was still relatively too sour and could not be appropriately enjoyed. The %EY obtained still needs to be increased to get a relatively more balanced espresso taste.

TABLE I. %EY PRELIMINARY TEST

Trial	Dose (gr)	Yield (gr)	Time (s)	%TDS	%EY
1	14	28.1	30	9.23	18.53
2	14	28.1	30	9.16	18.39
3	14	28.2	30	9.25	18.63
4	14	28.2	30	9.32	18.77
5	14	28	30	9.12	18.24
6	14	28	30	9.13	18.26
7	14	28	30	9.43	18.86
8	14	28.1	30	9.12	18.31
9	14	28.1	30	9.32	18.71
10	14	28	30	9.45	18.90
11	14	28	30	9.23	18.46
12	14	28.2	30	9.42	18.97
		Average			18.59

II. PRODUCT & LITERATURE REVIEW

A. *Product Review*

Entry-level espresso machines like the Delonghi have common components: water tank (45-53), vibration pump (79), overpressure valve (84), boiler (7,8,66,67), thermostat (4), and group-head valve. (9,10,14) [10]. Figure 1 shows the general components of the Delonghi espresso machine used by researchers in the test.

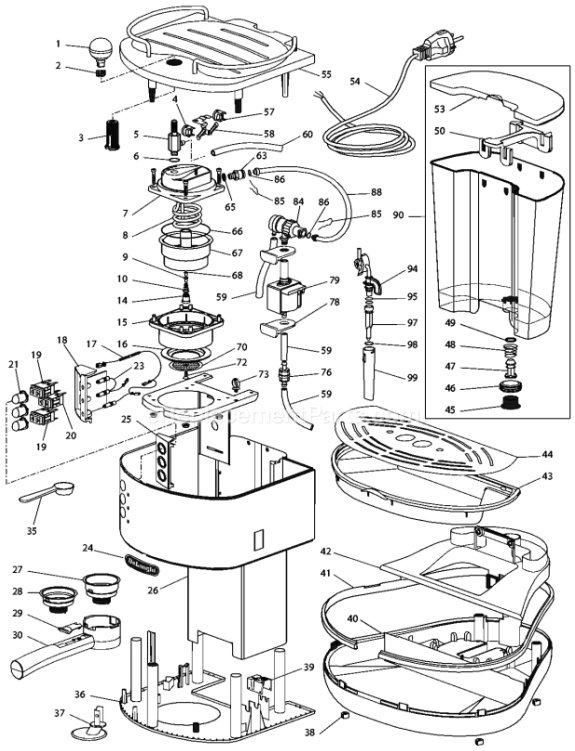

Fig. 1. Delonghi Components

Based on the researchers' observations, Figure 2 shows the structure of the circuit that composes the machine. When the engine is turned on, the boiler will immediately heat the water until it reaches the target temperature (105C) based on the thermostat attached to the outside of the boiler. The extraction process can be started by turning on the vibration pump that pumps water at room temperature from the water tank to the boiler. When the pressure in the boiler reaches 5bar, the group-head valve opens and lets water in the boiler come out for the extraction process. Between the water lines from the vibration pump and boiler, an overpressure valve will open when the pressure reaches 9bar to keep the extraction pressure from exceeding the limit.

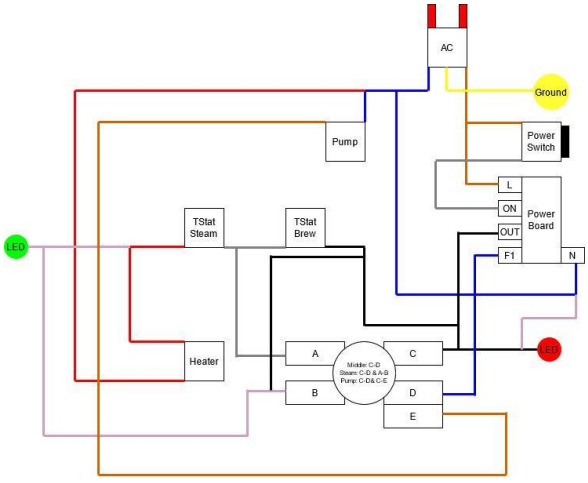

Fig. 2. Delonghi Wiring

B. *Literature Review*

Based on research [11], the water temperature used for the extraction process affects the ability of water to attract soluble contained in coffee bean particles. The higher the water temperature, the faster the extraction rate. If the soluble extraction is too low, the coffee will have a negative taste and disturbing acidity. However, if it is too high, some of the solubility, which has a negative taste, will also be extracted. Thus, to increase the extraction ability of an espresso machine properly, the temperature of the water used in the brewing process must be stable at the required number. Research [12] and [13] shows that the PID Control Algorithm can be used to maintain temperature stability well through its closed-loop design. PID Controller can maintain temperature stability better than a thermostat, which was only a relay based on the targeted temperature.

Research [14] shows dry coffee will have higher water resistance during the extraction process. While fully saturated coffee will be easier for water to pass through. Dry coffee flown by water with high pressure (9bar) has a higher possibility of channelling than fully saturated coffee. If channelling occurs, the extraction process in the basket will be uneven and have a lower extraction rate. Some parts of the coffee puck are highly extracted, while other parts don't. Reducing the coffee puck resistance and the risk of channelling can be done by flowing low-pressure/low flow rate water until the coffee is fully saturated before the primary extraction phase begin. This method is also called preinfusion. In research [15], the preinfusion phase can be done by controlling the speed of the vibration pump by adjusting the voltage given through the microcontroller.

C. *Hypothesis*

Based on the product and literature review related to the research problem, which is to improve the extraction ability of the espresso machine on coffee soluble. We will design two features that hypothetically can solve the problem:

1. Temperature Control Module with PID Controller: to increase water temperature stability as a replacement for the thermostat.
2. Flow Control Module: to regulate the speed of the vibration pump by adjusting the voltage resistance to reduce the water pressure/ flow rate used during the initial extraction at the preinfusion phase.

III. Solution & Testing Method

A. *Solution*

Figure 3 shows the new design of espresso machines that accommodate temperature control and flow control modules. Compared with Figure 2, the original design of a standard machine, there will be two main differences. The first difference lies in the two thermostats, which are no longer used and are replaced by a thermocouple probe with a PID Controller, which also functions as a Temperature Control module. The second difference was the addition of an AC Potentiometer to the circuit, which works as a Flow Control module to regulate the pump motor voltage of the espresso machine.

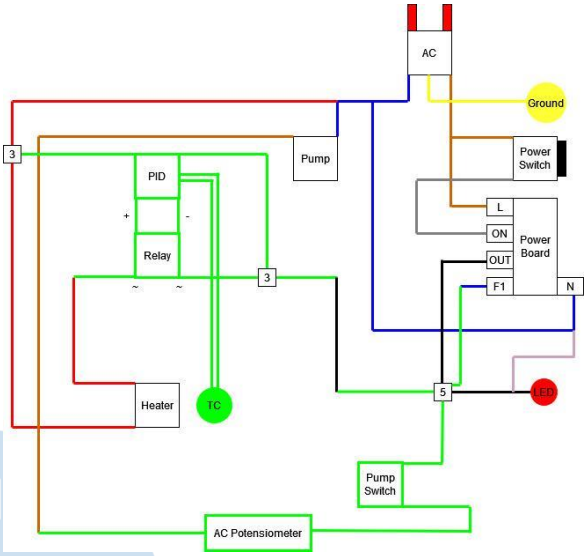

Fig. 3. New Wiring

In Figure 4 shows the internal parts of the espresso machine used. Researchers need to dismantle the inner frame that supports the boiler and pump motor to add the two modules.

Fig. 4. Boiler and Vibration Pump

In Figure 5 can be seen the final form of the machine that already has a temperature control and flow control module. The PID controller can regulate the water temperature in the boiler. Researchers used a water temperature of 115C in the boiler to produce a water temperature of 95C in the basket. The physical potentiometer knob can also adjust the motor speed on the vibration pump.

Fig. 5. The Final Build

Details of the removed parts:

- Steam wand and all of its connection pipes
- Brew/steam switch and all of its wiring
- Boiler's thermostat

Details of the added parts:

- PID controller and relay
- AC Potentiometer
- Two state switch
- 3D printed parts (front cover, module carrier, potentiometer's lever, switch bracket)

B. Testing Method

To measure the level of extraction, researchers used a refractometer from Atago [16], which can be seen in Figure 6; this tool can calculate the amount of soluble in coffee drinks. To measure the soluble coffee contained in espresso, we need to take a sample placed on the tool's lens to be measured. The measurement process occurs for a duration of 5 to 10 seconds. Ideally, the sample used has room temperature to maintain measurement consistency.

Fig. 6. Atago Refractometer

The extraction percentage calculation consists of the following steps:

- Measure the dose (D) of coffee used in grams.
- Measure the final espresso yield (Y) in grams.
- Measure the percentage of soluble coffee (TDS) successfully extracted at the final espresso yield using a refractometer.
- Measure the soluble gram (S) using the calculation: Y x TDS / 100
- Measure the percentage of extraction (%EY) that occurs by calculation: S / D x 100.

The test will begin by extracting 12 espressos (the maximum amount produced by the machine in 1 batch of water tanks) using the machine with added temperature control and flow control modules. The %EY will be measured on 12 espressos obtained, and the data will be compared with the previous preliminary testing data. Comparing the two data results will answer the research hypothesis of whether the two additional modules at the espresso machine can increase the machine's ability to extract soluble coffee in espresso drinks.

On the machine that has temperature and flow control modules, the brewing water temperature was set to 95C. As for the extraction profile, it uses the following steps:

- Do a pre-infusion for 20 seconds by setting the lowest water flow speed on the flow control module.
- Increase the speed of water flow through the flow control module until the end of the targeted extraction yield for 50 seconds. (The duration of 50 seconds was obtained from the calibration results based on the targeted yield amount. The calibration process was not described in detail in the report.).

IV. RESULT

The total data collection carried out by the researchers was 24 times for two test conditions, 12 times on a standard machine and 12 times on a machine that has added a temperature & flow control module. The amount of data collection was based on the maximum limit of espresso that both machines can produce in a fully filled water tank. Testing was based on conditions that were attempted to be close to the actual use situation.

The grind setting used in the test was based on the results of the researcher's dial with the highest possible %EY value target for each machine. The standard machine has a grind size that was relatively coarser than the modified machine. When the grind size on the standard machine was forced to be finer, the %EY did not increase. Instead, it decreases due to channelling in the puck.

The dose of coffee used in each test was 14 grams and was targeted to produce approximately 28 grams of espresso. The doses can be adjusted precisely but not with yield. It was challenging to ensure the yield would always be the same in every test due to the limitations of machines that still need to run and shut the pump manually.

Based on the test results, which can be seen in Table 2, the maximum %EY that can be achieved was 23.62%, with an average of 23.43% from 12 trials. Qualitatively, the espresso produced was more balanced than from the stock machine in the preliminary experiment. The intensity of the sourness in the under-extracted espresso has significantly reduced.

TABLE II. %EY FINAL TEST

Trial	Dose (gr)	Yield (gr)	Time (s)	%TDS	%EY
1	14	28.2	50	11.66	23.49
2	14	28.1	50	11.68	23.44
3	14	28.2	50	11.54	23.24
4	14	28	50	11.73	23.46
5	14	28.1	50	11.72	23.52
6	14	28.1	50	11.63	23.34
7	14	28.1	50	11.62	23.32
8	14	28	50	11.69	23.38
9	14	28	50	11.81	23.62
10	14	28.2	50	11.64	23.45
11	14	28	50	11.72	23.44
12	14	28	50	11.75	23.50
		Average			23.43

V. CONCLUSION

Based on the results of trials using an espresso machine that has added temperature control and flow control modules, there was an increase in the average percentage of extraction compared to the results of trials using stock machines; the average extraction percentage increased by 4.83 points. Qualitatively, this increase of %EY also significantly impacted the espresso taste, which tasted very sour and unbalanced, became relatively more balanced and comfortable to enjoy.

The research hypothesis was already answered, as shown in Figure 7, that adding temperature control and flow control modules on the Delonghi ECP33.21 espresso machine can increase the machine's ability to extract solubles from light roast coffee beans.

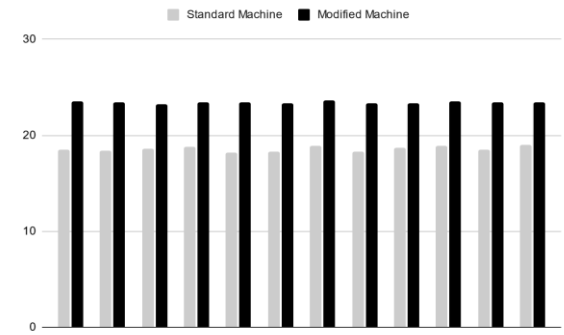

Fig. 7. %EY Comparison

ACKNOWLEDGEMENT

The author would like to thank Universitas Multimedia Nusantara for supporting this research by internal research funding program.

REFERENCES

[1] Spiro, M., and Selwood, R.M. (1984). The kinetics and mechanism of caffeine infusion from coffee: the effect of particle size. J. Sci. Food Agric. 35, 915–924.

[2] Spiro, M., and Page, C.M. (1984). The kinetics and mechanism of caffeine infusion from coffee: hydrodynamic aspects. J. Sci. Food Agric. 35, 925–930.

[3] Spiro, M., Toumi, R., and Kandiah, M. (1989). The kinetics and mechanism of caffeine infusion from coffee: the hindrance factor in intra-bean diffusion. J. Sci. Food Agric. 46, 349–356.

[4] Spiro, M. (1993). Modelling the aqueous extraction of soluble substances from ground roast coffee. J. Sci. Food Agric. 61, 371–372.

[5] Spiro, M., and Chong, Y.Y. (1997). The kinetics and mechanism of caffeine infusion from coffee: the temperature variation of the hindrance factor. J. Sci. Food Agric. 74, 416–420.

[6] Cordoba, N., Fernandez-Alduenda, M., Moreno, F. L., & Ruiz, Y. (2020). Coffee extraction: A review of parameters and their influence on the physicochemical characteristics and flavour of coffee brews. *Trends in Food Science & Technology*, *96*, 45-60.

[7] Spiro, M., and Hunter, J.E. (1985). The kinetics and mechanism of caffeine infusion from coffee: the effect of roasting. J. Sci. Food Agric. 36, 871–876.

[8] Cameron, M. I., Morisco, D., Hofstetter, D., Uman, E., Wilkinson, J., Kennedy, Z. C., Fontenot, S. A., Lee, W. T., Hendon, C. H., & Foster, J. M. (2020). Systematically Improving Espresso: Insights from Mathematical Modeling and Experiment. *Matter*, *2*(3), 631-648.

[9] Sunarharum, W.B., Williams, D.J., and Smyth, H.E. (2014). Complexity of coffee flavor: a compositional and sensory perspective. Food Res. Int. 62, 315–325.

[10] R. Parts, "Coffee Maker Parts," [Online]. Available: https://www.ereplacementparts.com/delonghi-eco310bk-coffee-maker-parts-c-122345_122351_122728.html. [Accessed 3 7 2021].

[11] Salamanca, C. A., Fiol, N., González, C., Saez, M., & Villaescusa, I. (2017). Extraction of espresso coffee by using gradient of temperature. Effect on physicochemical and sensorial characteristics of espresso. *Food Chemistry*, *214*, 622-630.

[12] Song, J., Cheng, W., Xu, Z., Yuan, S., & Liu, M. (2016). Study on PID temperature control performance of a novel PTC material with room temperature Curie point. *International Journal of Heat and Mass Transfer*, *95*, 1038-1046.

[13] Muhammad Asraf, H., Nur Dalila, K., Muhammad Hakim, A., & Muhammad Faizzuan Hon, R. (2017). Development of Experimental Simulator via Arduino-based PID Temperature Control System using LabVIEW. *Journal of Telecommunication, Electronic and Computer Engineering (JTEC)*, *9*(1-5), 53–57.

[14] Gagne, J. (2021). The Physics of Filter Coffee (Jonathan Gagné).

[15] Moss, Z. (2019). "Open Source Espresso Machine for Makers," University of Sheffield.

[16] V. Fedele, Universal refractometer apparatus and method, (2012), US Patent 8239144, filed Mar 31, 2010, and published Aug 7, 2012.

ISSN 2355-3286

Light Emiting Diode Control System based on the Microcontroller and Smartphone Application

Fahmy Rinanda Saputri[1], Lucia Blanca Rahawarin[2]
[1,2] Engineering Physics, Universitas Multimedia Nusantara, Tangerang, Indonesia
[1]fahmy.rinanda@umn.ac.id, [2]lucia.rahawarin@student.umn.ac.id

Accepted 07 October 2022
Approved 22 November 2022

***Abstract*— Nowadays, fulfilling the needs of human life requires costs. If the daily needs are under control, then the expense spent to meet the daily needs will also be controlled. In everyday electricity usage, the lights may turn on when the user does not need them. This incident resulted in a waste of electricity and costs. This research designs a Light Emitting Diode (LED) light control system using a microcontroller and smartphone application. The features available in the lamp control application consist of Off and On, Timer, Schedule, Electrical Energy Monitoring, and Automation based on Electricity Billing Budgeting. The tools and software used in the design of the lamp control are: Node MCU ESP8266 version 2, SRD-05VDC-SL-C relay module, ACS712 current sensor, Arduino IDE, MIT App Inventor, and ThingSpeak. The time delay from pressing the ON/OFF button on the smartphone until the light turns on is about 1-6 seconds. The error value for calculating the lamp power with the ACS712 current sensor against the lamp power from the specifications on the light box is 1.3%.**

***Index Terms*— Arduino IDE; Light Emitting Diode (LED); microcontroller; MIT App Inventor; ThingSpeak.**

I. INTRODUCTION

Based on the State Electricity Company (PT. PLN)'s Electricity Tariff Adjustment, the electricity tariff from October to December 2021 is Rp. 1,444,70/kWh [1]. In the daily electricity, lights may turn on even when the lights are not needed. This incident resulted in a waste of electricity and costs because the user still had to pay for the electricity used.

Electrical energy consumption at Lucia's house was recorded every day for four weeks. The electrical energy consumption data is visualized in the electricity consumption graph. The graph of electricity consumption per day is the total electrical energy consumption in 1 day. The graph of electricity consumption per 7 days is the electrical energy total consumption in 7 days starting from 7 days before the date written on the graph's axis. Fig. 1 and Fig. 2 are the graph of electricity consumption per day and seven days for four weeks at the Lucia's house.

In the first week, the use of electrical energy in the Lucia's house was carried out without any saving efforts or called business as usual. In the second to fourth week, saving attempts were made by turning off unused lights and electronics without compromising the comfort of the house occupants. Fig. 1 shows the trend line of daily electricity consumption at Lucia's house. From Fig. 2, the trend line in the use of electrical energy from the first to the fourth week is decreasing. The total electricity consumption in September 2021 is 115.9 kWh. Compared to electricity usage in the Lucia's house in August 2021, there is a decrease in the use of electrical energy by 15 kWh or 11.45%.

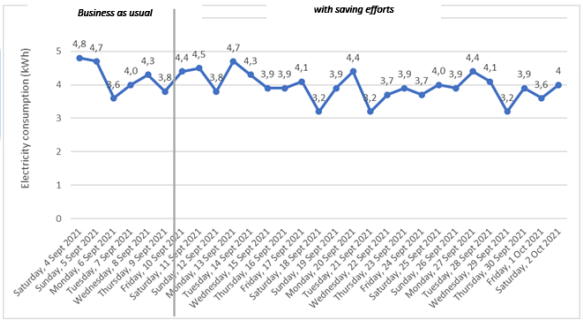

Fig. 1. Electricity Consumption per Day at Lucia's House

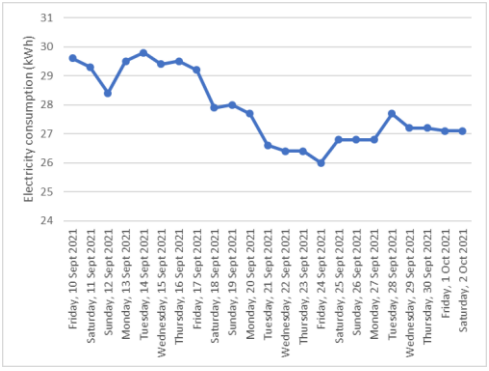

Fig. 2. Electricity Consumption per 7 Day at Lucia's House

Based on the previous research [2][3][4], Arduino and Bluetooth modules can control the lights on and off. ESP8266 Node MCU Wi-Fi module can also control light control via Wi-Fi [5]. In addition, Arduino can measure the use of electricity from an electronic device [6][7].

This research designs a light control system that can be set via a smartphone application to turn on and off automatically. In the smartphone application, there is a program to monitor the use of electrical energy for a light bulb and a program to calculate the duration of the lamp based on the user's electricity budget. Automation features based on monitoring energy and electricity budgets assist in knowing potential savings. In addition, no automation features for LED lamps have been found based on energy monitoring and electricity bill budgeting in the domestic market [8].

II. Materials and Tools

A. *Node MCU ESP8266 AMICA Wifi Module*

ESP8266 consists of a microcontroller (the part that controls) and TCP/IP (the part that connects to the internet). This chip can connect IoT devices to the internet via a Wi-Fi network by forming an embedded web server in the chip so that PCs and smartphones can connect to the ESP8266 chip [9].

In this research, the Node MCU used is the AMICA Node MCU (version 2) because it is smaller than Node MCU version 3. Node MCU is used to connect the circuit system to a wifi network so the user can control it via a wifi network.

B. *ACS712 20A Current Sensor*

The ACS712 Current Sensor is a sensor that can measure AC and DC from Allegro MicroSystems, Inc. The input voltage of this sensor is 5 V and will produce an output voltage in an analog form whose magnitude is proportional to the current being measured [10]. The current sensor ACS712 follows the working principle of the Hall Effect, where the sensor produces an output voltage that varies with the amount of current entering the sensor.

C. *Relay module SRD-05VDC-SL-C*

The relay module is an electrically operated electromagnetic switch. Like switches in general, a relay connects or disconnects the flow of electric current. Relay can be controlled by low voltage rated at 3.3 V and high voltage rated at 12 V, 24 V, and even mains voltage (230 V European standard or 120 V American standard) [11]. This research uses relay SRD-05VDC-SL-C due to this is the easiest to find in the market online during the making of this work.

D. *Others*

The other materials and tools used in this work are Light Emitting Diode (LED) 3W as the object to be controlled, transparent cable, bras plug, and FK 218 lighting as a lamp holder.

E. *Arduino IDE*

Arduino IDE software can run on Windows, Macintosh, OSX, and Linux operating systems. This software appears as an open-source device open to an experienced programmer's development. In this research, Arduino IDE software is essential in setting the Node MCU. Then, The LED can be controlled by it.

F. *MIT App Inventor*

This block-based programming software facilitates the creation of complex applications in much less time than in traditional programming environments. The MIT App Inventor project aims to develop software by empowering everyone, especially young people, to move from technology consumption to technology creation [12]. In this research, MIT App Inventor plays an essential role in designing and application coding on the smartphone for the light controller.

G. *ThingSpeak*

ThingSpeak is an IoT analytics platform that can aggregate, visualize and analyze data flows live from Cloud storage. In this research, ThingSpeak provides a fixed website link so that the user does not need to be periodically replaced the embedded web server link in the form of IP addresses that change frequently. ThingSpeak also visualizes sensor data in graphical and numerical form in real-time.

III. Design Methodology

A. *System Design Overview and Workflow*

Fig. 3 is the flowchart of lighting control design system's overview and workflow.

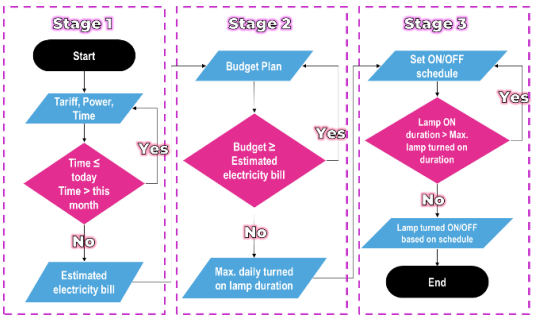

Fig. 3. System Design Flowchart

In stage 1, the user is directed to input the electricity tariff (Rp./kWh), lamp power (W), and automation period. Automation time cannot be less than today and more significant than this month. The user must re-enter

the automation time range if the conditions are not met. The output of this stage is the estimated electricity bill when the lights are turned on continuously for 24 hours.

In stage 2, the user is directed to enter a budget plan. The user must re-enter the budget plan if the budget plan exceeds the estimated electricity bill calculated in the first stage. The output of the second stage is the maximum duration of the lights per day.

In stage 3, the user is directed to set a schedule for turning off the lights for 24 hours. This schedule will be applied daily within the automation time range inputted in stage 1. The lights' duration cannot be greater than the maximum duration of the lights, which is calculated in stage 2. If the schedule meets the requirements, the lights will start turning off according to the specified schedule.

B. System Block Diagram

The block diagram, as shown in Fig. 4, shows the main component of the control system design. The LED light is connected to the ACS712 current sensor and relay module SRD-05VDC-SL-C. The ACS712 current sensor sends input to the Node MCU in the form of a voltage which will be translated into LED lamp current. The relay module receives output from the Node MCU in the form of a voltage to regulate the LED lights on and off. The Node MCU sends on-off commands and reading of ACS712 sensor data to web server ThingSpeak via the internet. Commands and data stored in ThingSpeak are then sent to the app smartphone through the internet network.

Fig. 4. System Design Block Diagram

C. Testing Method

- LED On/Off Program via Smartphone Application

1) The Circuit

The ESP8266 Node MCU output voltage, which is 3.3V-5V DC, cannot be used to turn on a 3 Watt LED lamp whose input voltage is 170V-250V AC. Therefore, the first step is to make a simple electrical circuit that can power a 3 Watt LED lamp, consisting of the E27 lamp holder, cable, and an EU plug. Then the relay module must be added in circuit. Fig. 5 is the schematic of circuit with relay module.

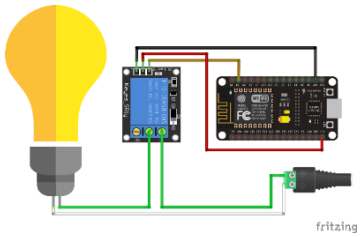

Fig. 5. Circuit Plus Relay Module Schematic

2) Application Display

The circle button labelled "OFF" or "ON" functions to turn the light off when pressed. If the button is dark gray and says “OFF” is pressed, the button will change color to light gray with the words “ON” and the light will turn on about 1-6 seconds later. As long as the “ON” button is light gray, the button cannot be pressed for 20 seconds. There is timer below the screen that says “Please wait for … seconds” to indicate how many seconds have passed since the button was pressed. After 20 seconds, the “ON” button will turn yellow.

When using an IP address as a web server, lights can immediately turn off or on after the ON / OFF button in the application is pressed. The time range of about 1-6 seconds when using ThingSpeak as the web server is because the path of sending commands to the IP address is shorter than to ThingSpeak, an intermediary platform. Using ThingSpeak, once the Node MCU is connected to the IP address, Node MCU commands are passed to the web server ThingSpeak and then forwarded to channel-specific target.

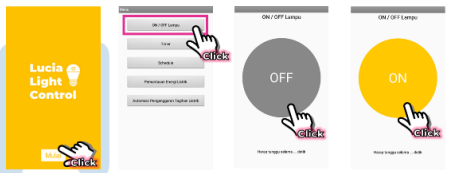

Fig. 6. Light’s ON/OFF Menu Display

- LED On/Off with Timer Program

The LED light can be turned ON/OFF by a timer. Hours, Minutes and Seconds settings by the user will be counted down. If the button Start is pressed, the countdown timer at the bottom of the app will continue to decrease every 1 second. If it reaches 00:00:00, the light will turn off if the circle button is set to “OFF”, or the light will turn on if the circle button is set to “ON”.

Fig. 7. Timer Menu Display

- LED On/Off with Schedule Program

The schedule is the LED on and off scheduling feature. First, press the “Select Time” button. After selecting the time, press the “Lamp Condition” button to set whether you want to schedule the lights to turn on or off at the selected time.

Fig. 8. Schedule Menu Display

After setting the time and condition of the lights, press the "Add" button then the scheduling will be carried out. The caption “Currently there are… scheduling” will be updated according to the many schedules that have been added after pressing the "Add" button or deleted after the schedule you want to delete is selected, and then the "Delete" button is pressed.

- Electrical Energy Monitoring Program

1) The Circuit

After the relay module turns off the lights, an ACS712 current sensor is added to the circuit. ACS712 current sensor is installed in series after the relay module. Fig. 9 is the schematic of the circuit after is added by the ACS712 current sensor.

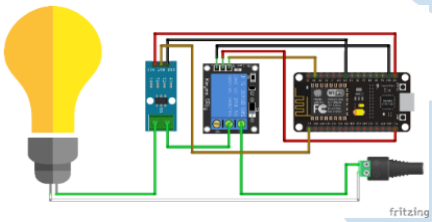

Fig. 9. Circuit Plus ACS712 Current Sensor Schematic

2) Application Display

This menu has a numeric display of energy used, a numeric display of lamp power, an energy graph, and a power graph that updates every 20 seconds. The ACS712 current sensor data is processed in the Arduino IDE and then sent to the ThinkSpeak web server. Next, ThingSpeak will visualize the ACS712 sensor data in graphic form and show the ACS712 sensor data in a numeric display. The display of numbers and graphs from ThingSpeak is then entered into the MIT App Inventor to view the data visualisation through the smartphone application.

Fig. 10 displays the Electrical Energy Monitoring menu when the lamp is on. metersis the total electrical energy that the lamp has used. Power Meter shows the power of the lamp when the lamp is on, which is 3.01 W. The Energy Graph line shows the energy value increase when the lamp is turned on. The line on the Power Graph indicates the power rating is around 3 Watts when the lamp is on.

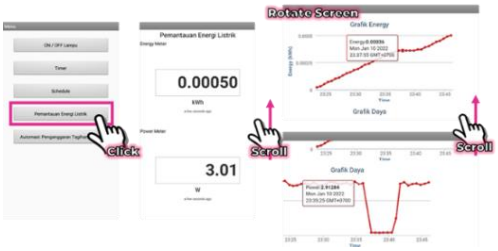

Fig. 10. Electrical Energy Monitoring Menu Display When LED ON

Then, Fig. 11 displays the Electrical Energy Monitoring menu when the lights are off. Energy Meter is the total electrical energy that the lamp has used. The power meter shows how much power the lamp has when the lamp is off, which is 0.28 W. The line on the Energy Graph tends to be flat when the lamp is turned off. The line on the Power Graph shows the power rating is around 0 Watt when the lamp is off.

Fig. 11. Electrical Energy Monitoring Menu Display When LED OFF

- Automation Feature Based on Electricity Bill Budgeting Program

1) Stage 1: Input PLN Electricity Basic Tariff, Lamp Power, and Automation Time Range

PLN's basic electricity tariff is inputted according to the ongoing PLN stipulation. The input lamp power figures can be referenced from the specifications on the lamp box or lamp power calculations in the application. Minimum automation time starts at 00:00. If 00:00 has passed, the automation can be started for the next day. The maximum automation time is the end of the same month as the automation start date. If "Select Start Date" and "Select End Date" do not match the conditions described previously, a warning message will appear, and the "Submit" button cannot be pressed.

If the start date and end date are by the program provisions, then the "Submit" button can be pressed. When the "Submit" button is pressed, a "Check Input" will appear to ensure the user's input TDL, power, and automation time is correct. In addition, a "Calculation" will appear where users can see the duration of the day, the automation time, and the estimated electricity bill.

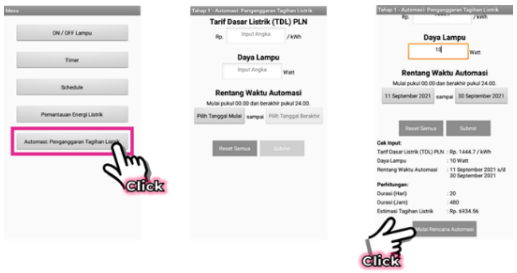

Fig. 12. Automation Menu Display - Stage 1

2) Stage 2: Input the Budget Plan

At the top of the application screen there is a summary of user input in previous stage. Next the user can enter the budget plan figures. If the user's budget plan input is greater than the estimated value of the electricity bill, a warning message will appear and the "Light Scheduling per Day" button will not appear. If the user's budget plan input is less than the estimated value of the electricity bill, a "Calculation" and "Light Scheduling per Day" button will appear to proceed to the next stage. In the “Calculation” section, users can see how long the lights are on per day according to the user's budget.

Fig. 13. Automation Menu Display - Stage 2

3) Stage 3: Light Scheduling per Day

At stage 3, you can see the buttons are rectangular in shape with the words "OFF". These buttons are worth 1 hour calculated from the hour on the top left of the buttons. If these buttons are pressed by the user, then the button pressed will read “ON” and the “Total Light On Time” will increase. If the buttons that say "ON" are pressed again, the writing on the button will change to "OFF" and "Total Light Time On" will decrease.

Fig. 14. Automation Menu Display - Stage 3

At the bottom of the ON/OFF buttons, there is a “Check” button. If “Total Lamp On Time” is less than “Max. Duration of Lights On/ Day”, there will be a message informing you of the difference in costs from the input of the previous budget plan. If “Total Lamp On Time” is greater than “Max. Duration of Lights On/Day”, there will be a warning message. The “Create Schedule” button can be pressed if “Total Light On Time” is less than or equal to “Max. Lamp Light Duration/Day”. After pressing the “Create Schedule” button, a schedule of lights will appear at the bottom of the screen. If we scrolldown, we will find the "Start Automation" button. After pressing the “Start Automation” button, the schedule that has been made in stage 3 of the Automation menu will be sent to the Schedule menu. It appears that there are now 24 scheduling lights that will be implemented. Thus, the lights will turn off according to the schedule.

IV. Result and Analysis

A. Measurements and Calculations

- NodeMCU Output Voltage: VIN, 3.3V, GPIO5 Pins

To select which Node MCU pins are suitable to use by the 05VDC-SL-C relay module and ACS712 current sensor, the output voltage of the Node MCU pins is measured. Table I shows the measurement results for the VIN, 3.3V, and GPIO5 Node MCU pins using a multimeter.

TABLE I. Node MCU Output Voltage Measurement

Pin Node MCU	Measurement to-										
	1	2	3	4	5	6	7	8	9	10	Mean
VIN (V DC)	4,75	4,75	4,76	4,76	4,76	4,76	4,76	4,76	4,76	4,76	4,76
3.3V (V DC)	3,28	3,30	3,30	3,30	3,30	3,30	3,30	3,30	3,30	3,30	3,30
GPIO (V DC)	3,28	3,28	3,28	3,28	3,28	3,27	3,27	3,27	3,27	3,27	3,28

Based on measurements, it is using a multimeter, the average output voltage of the VIN pin = 4.76V, the 3.3V pin = 3.3V, and the GPIO5 pin = 3.28V. The input

voltage of the relay module 05VDC-SL-C and the current sensor ACS712 is 5VDC, while based on measurements, no Node MCU pin produces an output voltage of 5VDC. The solution is better to use a 5VDC relay module equipped with an optocoupler so that it can still be controlled by the Node MCU with a voltage of less than 5VDC. The selection of the Node MCU pins for the ACS712 current sensor will be calculated through the following calculations.

- Zero Current Output Voltage ACS712: VIN, 3.3V Pins

Zero current output voltage is generated by the ACS712 current sensor when no electricity is flowing to turn on the lamp.

TABLE II. ZERO CURRENT OUTPUT VOLTAGE MEASUREMENT

VCC	Tools	Unit	Measurement to-										
			1	2	3	4	5	6	7	8	9	10	Mean
VIN	Multimeter	VDC	2,37	2,38	2,37	2,38	2,38	2,35	2,35	2,36	2,36	2,36	2,37
	Arduino IDE	Analog	801	802	801	800	800	797	797	797	798	798	799
		VDC	3,72	3,73	3,72	3,72	3,72	2,58	2,58	2,57	2,57	2,58	3,15
3.3V	Multimeter	VDC	1,63	1,63	1,63	1,63	1,63	1,62	1,62	1,62	1,62	1,62	1,63
	Arduino IDE	Analog	549	547	547	548	549	545	545	544	544	545	546
		VDC	1,77	1,76	1,76	1,77	1,77	1,76	1,76	1,76	1,76	1,76	1,76

Next is to compare the zero current output voltage measurement results from Arduino IDE with zero current output voltage based on the formula. According to the theory, if no current flows through IP+ and IP- or the current is equal to zero, then the output voltage of the ACS712 sensor will show VIOUT = VCC × 0.5 [13]. The error in this calculation is how far the zero current output voltage value is based on Arduino IDE from the zero current output voltage value based on the VIOUT formula. The following is the calculation of the theoretical VIOUT and the error of measured VIOUT with ACS712 against theoretical VIOUT:

1) $VIOUT_{VIN\ theoretical} = VCC_{VIN\ [Table\ 4]} \times 0{,}5$

$= 4{,}76 \times 0{,}5$

$= 2{,}38V$

$VIOUT_{VIN\ measured\ [Table\ 5\ with\ Arduino\ IDE]} = 3{,}15V$

$Error = \frac{|VIOUT_{meas.} - VIOUT_{theo.}|}{VIOUT_{theo.}} = \frac{|3{,}15 - 2{,}38|}{2{,}38} = 0{,}32$

2) $VIOUT_{3.3V\ theoretical} = VCC_{3.3V\ [Table\ 4]} \times 0{,}5$

$= 3{,}3 \times 0{,}5$

$= 1{,}65V$

$VIOUT_{VIN\ measured\ [Tabel\ 5\ with\ Arduino\ IDE]} = 1{,}76V$

$Error = \frac{|VIOUT_{meas.} - VIOUT_{theo.}|}{VIOUT_{theo.}} = \frac{|1{,}76 - 1{,}65|}{1{,}65} = 0{,}06$

According to the specification sheet, the ACS712 current sensor's input voltage is 5V. The VIN=4.76V pin voltage is closer to 5V than the 3.3V=3.3V pin. However, the error of VIOUT in the 3.3V pin is smaller than the VIOUT in the VIN pin. By looking at this calculation, the 3.3V pin is decided to be the voltage source for the ACS712 current sensor.

B. System Design Overview and Workflow

- Electrical Energy Monitoring Menu

The ACS712 current sensor measures the electric circuit's current flow by calculating the sensor's potential difference or output voltage. The output voltage of the current sensor mounted on pin A0 Node MCU is first displayed in analog form bit 0-1024 by Arduino IDE. The mathematical equation for converting analog data into sensor voltage (V sensor) is:

$$V\ sensor = Analog\ Data\ (bit) \times \frac{3{,}3\ V}{1024\ (bit)} \quad (5)$$

Analog data is obtained from analogRead(A0), 3.3 V from the maximum ADC of the Node MCU, and 1024 is the maximum analog data that the Node MCU can measure. Next, the V sensor is translated into sensor current (I sensor) using the following mathematical equation:

$$I\ sensor = \frac{V\ sensor\ (V)}{0{,}1\ V/A} \quad (6)$$

V sensor is obtained from equation (5), and 0.1V/A is obtained from the current sensor sensitivity of ACS712 20A. If using the ACS712 5A, then the sensitivity is 0.185 V/A. If you use the ACS712 30A, the sensitivity is 0.66 V/A.

After getting the circuit current, the next step is to find the lamp voltage. Inside the 3W LED, there is an MB10F rectifier. The MB10F rectifier specification shows that the voltage drop for every 0.4A is 1V [14]. So, the mathematical equation for the lamp voltage is as follows:

$$V\ Lamp = I\ Sensor\ (A) \times \frac{1V}{0{,}4A} \quad (7)$$

The lamp power calculation is the circuit current multiplied by the lamp voltage. Here is the mathematical equation:

$$Power\ (W) = I\ Sensor\ (A) \times V\ Lamp\ (V) \quad (8)$$

Finally, the calculation of energy is power times time. This series updates energy calculation every 20 seconds. Here is the mathematical equation:

$$Energy(kWh) = Power(W) \times \frac{1kW}{1000W} \times 20s \times \frac{1h}{3600s} \quad (9)$$

- Automation Menu:Electricity Bill Budgeting - Stage 1

The first input is TDL (Rp./kWh), lamp power (W), and automation period (days). If the next buttonSubmitpressed, it will display “Check Input” to ensure the user input is correct and “Calculation” will also appear. At this stage, the application calculates the duration (days), duration (hours), and estimated electricity bills. Here is the mathematical equation of the calculations in the first stage:

$$Duration\ (Day) = End\ Date - Start\ Date \quad (10)$$

$$Duration\ (Hour) = Duration\ (Day) \times \frac{24\ Hour}{1\ Day} \quad (11)$$

$$Estimated\ Electricity\ Bill = \frac{TDL\ (Rp./kWh) \times Duration(h) \times Power(W) \times 1\ kW}{1000W} \quad (12)$$

- Automation Menu:Electricity Bill Budgeting - Stage 2

The budget plan is entered into the column provided, then click Submit. Next is the calculation of duration (days), duration (hours), and the length of time the lights are on (hours/day).

$$Duration\ (Hour) = \frac{Budget\ Plan(Rp.)}{TDL\ (Rp./kWh)} \times \frac{Power(W) \times 1kW}{1000\ W} \quad (13)$$

$$LED\ ON\ \left(\frac{Hour}{Day}\right) = \frac{Duration\ (Hour)}{Duration\ (Day)} \quad (14)$$

- Automation Menu:Electricity Bill Budgeting - Stage 3

At this stage, the user enters a schedule for turning off the lights as many times as the lights are on per day calculated in the previous stage. The total duration of the lights on must be less than or equal to the length of time the lights are on per day. Here is the mathematical equation for this condition:

$$LED\ ON\ Duration\ Total \leq Max.LED\ ON\ per\ Day\ Duration \quad (15)$$

- Energy Monitoring with ThingSpeak

Current measurements from current sensors and lamp voltage calculations, lamp power, and lamp electrical energy come from the Arduino IDE and are then sent by the Node MCU to ThingSpeak. Fig. 15 is a graph of the current, voltage, power, and electrical energy of the lamp when it is turned on.

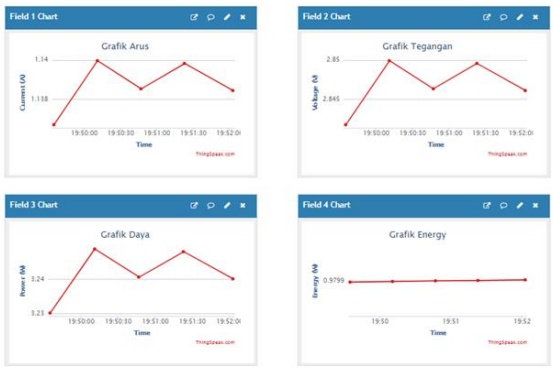

Fig. 15. Current, Voltage, Power, and Energy When LED ON Graphs

TABLE III. CURRENT, VOLTAGE, POWER, ENERGY WHEN LAMP IS ON

Lamp is ON	Measurement to-										
	1	2	3	4	5	6	7	8	9	10	Mean
Current (A)	1,14	1,14	1,14	1,14	1,14	1,14	1,14	1,05	0,98	1,02	1,10
Voltage (V)	2,85	2,85	2,85	2,84	2,84	2,84	2,85	2,62	2,46	2,34	2,73
Power (W)	3,25	3,24	3,25	3,24	3,22	3,23	3,24	2,74	2,41	2,57	3,04
Energy (Wh)	0,02	0,02	0,02	0,02	0,02	0,02	0,02	0,02	0,02	0,02	0,02

When the light is on, the average power calculated by the program is 3.04W. The lamp power based on the specifications on the box is 3W. If the calculated power of the program is compared with the lamp power of the specification, the error value of the calculated power is:

$$Power\ Calculation\ Error = \frac{|3{,}04 - 3{,}00|}{3{,}00} \times 100\% = 1{,}3\% \quad (16)$$

This value shows the difference in the measurement of the lamp power value using the ACS712 current sensor with the lamp power value in the lamp specification. Fig. 16 is a graph of the current, voltage, power, and electrical energy of the lamp when it is turned off.

When the light is off, the average power calculated by the program is about 0.01W. The current, voltage and power graph drops near 0 when the lamp is turned off. However, the energy graph does not go down because the energy graph is the total energy since the first time the lamp is turned on.

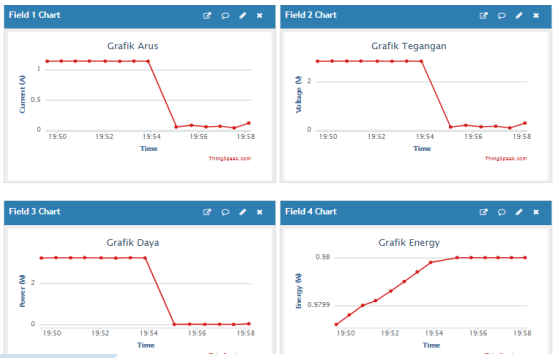

Fig. 16. Current, Voltage, Power, and Energy When LED OFF Graphs

TABLE IV. CURRENT, VOLTAGE, POWER, ENERGY WHEN LAMP IS OFF

Lamp is OFF	Measurement to-										
	1	2	3	4	5	6	7	8	9	10	Mean
Current (mA)	53,71	81,52	57,00	66,19	39,38	39,38	19,06	49,67	87,83	90,50	58,42
Voltage (mV)	134,28	203,80	142,50	165,47	98,45	98,48	47,65	124,18	219,57	226,26	146,06
Power (mW)	7,21	16,61	8,12	10,95	3,88	3,88	0,91	6,17	19,29	20,48	9,75
Energy (kWh)	0	0	0	0	0	0	0	0	0	0	0

V. CONCLUSION

The lamp turned on and off via Node MCU through a smartphone application designed from web-based software programming, MIT App Inventor. The Node MCU is connected to the smartphone application through the ThinkSpeak web server. Period from ON/OFF button pressed on the smartphone until the light is ON/OFF for about 1-6 sec. Lamp's power calculation error using the current sensor against the power of lamp specification is 1.3%.

ACKNOWLEDGEMENT

We thank Universitas Multimedia Nusantara, which provides the whole necessary for this research.

REFERENCES

[1] PT PLN (Persero), "Electricity Tariff - PT PLN (Persero)," 2021.[Online].Available:https://web.pln.co.id/pelanggan/tari

f-energi-listrik/tariff-adjustments. [Accessed September 20, 2021].

[2] F. Rahmadayanti, "Arduino-Based LED Lamp Android Application," 2016.

[3] M. Hudori and Y. Paisal, "Design of Automatic Lighting Control System in Residential Houses to Increase Electricity Consumption Efficiency," 2019.

[4] E.T. Setiawan, "Controlling Home Lights Based on Arduino Microcontroller Using Android Smartphone".

[5] J. Chandramohan, R. Nagarajan, K. Satheeshkumar, N. Ajithkumar, PA Gopinath and S. Ranjithkumar, "Intelligent Smart Home Automation and Security System Using Arduino and Wi-fi," 2017.

[6] M.I.L. Wahyu, Syaifurrahman and M. Saleh, "Design of a Digital kWh Meter as a Cost Calculator of Electrical Energy Usage Based on Arduino UNO R3".

[7] G. Herandy and M. Suprianto, "Monitoring of Costs and Measurement of Electric Power Consumption Based on Arduino Mega2560 Using the Web," 2019.

[8] L.B. Rahawarin, "Comparative Study of Data and Innovation Ideas for Automation Features of Smart Home Products PT. BARDI Automation Solutions," UMN Knowledge Center, Tangerang, 2021.

[9] E. Ouyang, "Introduction," in *Hands-On ESP8266: Mastering Basic Peripherals*, Hands On Embedded, 2018, pp. 1-4.

[10] A. Roman, "A Simple Approach to Measure ACDC," March 25, 2020. [Online]. Available: https://www.romn.io/2020/05/a-simple-approach-tomeasure-acdc.html. [Accessed September 21, 2021].

[11] R. Santos, "ESP8266 NodeMCU Relay Module – Control AC Appliances (Web Server)," Random Nerd Tutorials, December 18, 2019. [Online]. Available: https://randomnerdtutorials.com/esp8266-relay-module-ac-webserver/. [Accessed September 22, 2021].

[12] MIT App Inventor, "About Us - MIT App Inventor," Massachusetts Institute of Technology, [Online]. Available: https://appinventor.mit.edu/about-us. [Accessed September 22, 2021].

[13] Allegro MicroSystem, "Fully Integrated, Hall-Effect-Based Linear Current Sensor IC with 2.1 kVRMS Isolation and a Low-Resistance Current Conductor," [Online]. Available: https://pdf1.alldatasheet.es/datasheetpdf/view/205336/ALLEGRO/ACS712.html. [Accessed September 21, 2021].

[14] PACELEADER [PACELEADER INDUSTRIAL], "Miniature Glass Passivated Single-Phase Surface Mount Flat Bridge Rectifier," [Online]. Available: https://pdf1.alldatasheet.com/datasheet pdf/view/310355/PACELEADER/MB10F.html. [Accessed September 24, 2021].

ISSN 2355-3286

Semi-Automatic Medical Syringe Pump Development: Interface, Control, Alarm, and Feedback

Kevin Nicholas Tanex[1], Megantara Pura[2]
[1,2] Electrical Engineering, Universitas Multimedia Nusantara, Tangerang, Indonesia
[1]kevin.tanex@gmail.com, [2]megantara.pura@umn.ac.id

Accepted 18 October 2022
Approved 22 November 2022

***Abstract*— The syringe pump is used to inject liquids for a long period of time and on a small volume scale. The presence of air inside the hose whilst injection into the human body is dangerous. Early detection can be done using a bubble sensor. The SPICAF is equipped with a gearbox capable of injecting long-term injections on a small scale, and a bubble sensor capable of detecting air by comparing light intensity on a clear hose which automatically notifies the user if dangerous conditions occur. The SPICAF is successfully designed, developed, and tested to WHO specifications. It's injection has 98% accuracy and is able to detect air bubbles properly.**

***Index Terms*— automatic; bubble sensor; gearbox; injection; injection pump.**

I. Introduction

Some diseases experienced by a patient require regular treatment and need to be observed by health workers gradually and periodically [1]. In one treatment process, health workers need to periodically give medicine to patients, it can be in the form of solid or liquid drugs [2]. One way to give liquid medicine is by injection method. The injection process transfers liquid drugs into the human bloodstream [3]. Drugs that are injected include insulin or other hormones, antibiotics, chemotherapy drugs, and pain relievers [4]. The injection method is usually done manually by health workers using injections or automatically using tools. One of the tools that can perform injection automatically is a syringe pump [5]. The automatic injection can lighten the workload while reducing the risk of inaccuracy by health workers [6]. During the injection process, the presence of air that enters the human bloodstream is called an anomaly of air embolism [7]. Embolism is a condition in which the presence of air in the blood circulation causes obstruction of blood flow [8]. Blood supply is blocked due to embolism can cause major human organs such as the brain, heart, and lungs to experience blood deficiency [9]. In the worst case, blood deficiency causes organ failure and death [10].

From the preceding context, this study aims to develop a syringe pump that can operate automatically and prevent air from entering the human blood circulation by detecting it before proceeding with the injection. Researcher chose to develop a syringe pump because the response time is more stable than peristaltic pumps and more affordable than pressure-driven pumps. Syringe pumps can perform injections on a very small scale, accurately, and at a specific speed. [11]. Previous study has developed a technique for detecting air inside human blood, employing a capacitive sensor method to identify bubbles, which was detected after the hemodialysis process [12]. Other research uses the triple modular redundancy (TMR) method in their sensors to make a fault tolerant air bubble detector [13]. The created syringe pump in this study takes a novel approach to the problem. It has a luxmeter-based bubble sensor module that detects bubbles in the injection hose and can take input from health staff so that it may operate autonomously. Sensor readings are used as feedback to be processed and notify health workers if there are problems during operation. The developed syringe pump system is called SPICAF (Syringe Pump: Interface, Control, Alarm, and Feedback). In conclusion, SPICAF is able to deliver injection accurately at given flowrate and is able to check for any air bubbles inside its hose.

II. Research Method

A. Design Concept

The process of making SPICAF follows the standard syringe pump specifications from WHO (World Health Organization) [14]. SPICAF is composed of hardware, electronic components, and software. The SPICAF structure is made of acrylic board and MDF (Medium-Density Fiberboard) which are connected using elbows and hinges. Some hardware components are made using a 3D (three-dimensional) printer while others are purchased. Electronic components include keypad, LCD (Liquid Crystal Display), LED (Light Emitting Diode), luxmeter BH1750 module, buzzer, stepper motor, stepper motor driver, microcontroller, micro SD (Secure Digital) card module, ATS (Automatic Transfer Switch), batteries,

adapter, and step-up module. The following are the results of the development of SPICAF.

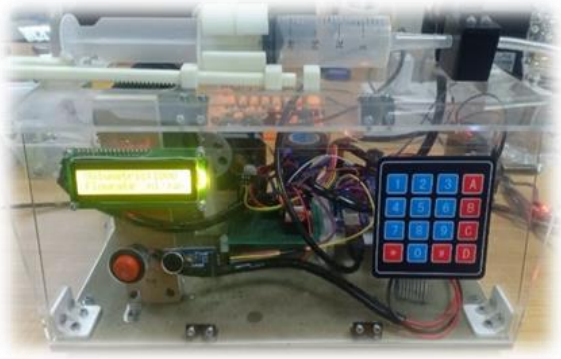

Fig. 1. SPICAF Front View

From the design above, how to use SPICAF to be developed can be described as follows.

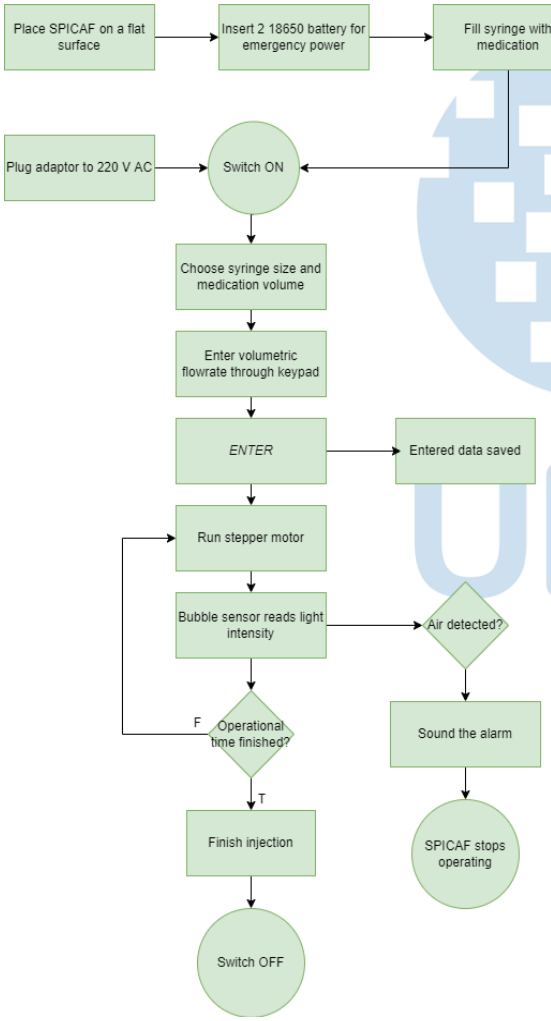

Fig. 2. SPICAF Flowchart

B. Subsystem

The SPICAF system consists of several subsystems connected to the microcontroller. The subsystem consists of hardware and electronic components, some of which are run using Arduino IDE (Integrated Development Environment)-based software.

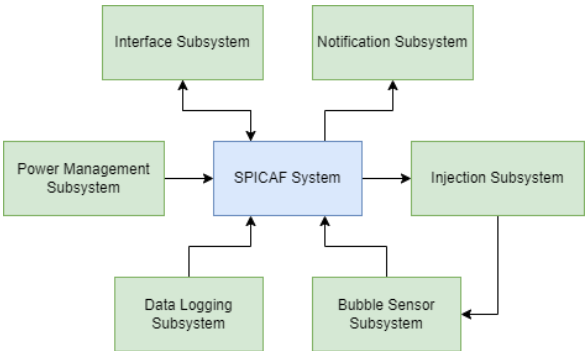

Fig. 3. Diagram of the subsystems on SPICAF

The interface subsystem interacts with the user through the 4x4 keypad and LCD components. This subsystem serves to receive user input and show the results of the input to the user.

The user notification subsystem functions to notify the condition of the SPICAF when operating, whether it is normal or experiencing problems. Notifications are notified via the LCD and buzzer.

The data logging subsystem is a subsystem that will store the input results and the results of calculations entered by the user into the micro-sd card via the micro SD card module.

The injection propulsion subsystem will drive the syringe to perform the injection. The driving component uses a stepper motor connected to a gearbox and rack and pinion which converts rotational motion into linear motion [15]. The stepper motor used is NEMA 17 which is controlled using the A4988 stepper motor driver. The reading of the rotational speed of the stepper motor uses a digital rotary encoder in rpm (rotation per minute).

The bubble sensor subsystem functions to detect air during the injection. Detection is done by comparing the difference in light intensity of the clear hose and the liquid-filled hose [16]. The light is emitted by the LED and measured by the BH1750 in a closed black box. Light intensity is in lux units.

With the subsystems above, SPICAF has some features and spesifications which fullfills some of the WHO standard criterias, includes:

- Automatic data logging
- Bubble detection
- Softstarter implementation
- Temporary back-up power
- User interface to receive and show input
- User notification with alarm sound not less than 45 dB
- Stepper motor rotation speed from 1 to 300 rpm, which translates to volumetric flowrate injection of 3600 nl/hour – 1080000 nl/hour

III. ANALYSIS

A. *Bubble Sensor Subsystem*

Air bubble sensor is used to detect the precence of air inside a vessel. Research [12] uses platinum plates to create the capacitor sensor. In their experiment, they used Dextran70 solution to simulate blood. Their sensor outputs certain voltage to detect the air bubbles. On the other hand, research [13] also uses capacitive sensor with TMR implementation. It incorporates a voting technique into the voter circuitry at the end of their sensors to guarantee that they all work together and get the same input signal. This ensures their air bubble detector is accurate and prevents sensor errors, especially if sensors fail to function properly.

The bubble sensor subsystem in this setup detects air by comparing the difference in light intensity when it is filled with air or liquid in a clear hose. The bubble sensor is positioned just after syringe's tip. In contrast to the previous studies, this setup merely employs LED, a black box, and a BH1750 luxmeter. Light is emitted by the LED. Light intensity is then measured by BH1750 sensor in lux unit [17] inside a black acrylic box measuring 2 x 4 x 3 cm^3. BH1750 is a digital ambient light sensor IC for I2C bus interface. Measurement of light intensity is carried out using a *millis()* based timer from the Arduino IDE. The measurement is carried out in a well-lit laboratory. The syringe hose is then filled with water or air as an experiment limitation.

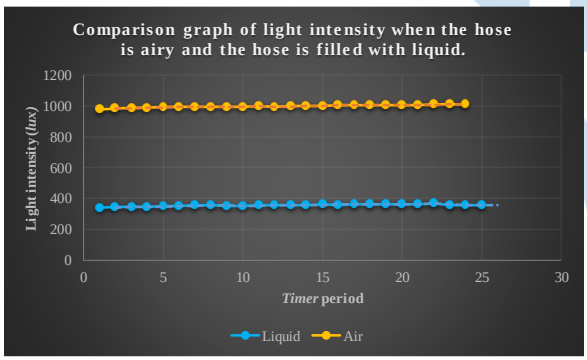

Fig. 4. Graph of measuring the intensity of light when the hose is airy and the hose is liquid

It is worth noting that the hose has a diameter of 5 mm. Outlier data is ignored from the statistical calculation of the data. In air condition, the data has a mean of 996,4132 lux with a maximum of 1009 lux, while in liquid condition, the mean is 355,1332 lux with a maximum of 365 lux. If sensor reads more than 365 lux, it indicates the existence of trapped tiny air bubbles during injection. By comparing these results, it is possible to deduce that as long as the bubble sensor detects a light intensity of less than 365 lux, the subsystem does not detect air and the SPICAF runs normally without any bubble inside its hose.

B. *Injection Subsystem*

The injector subsystem drives the injection via a gearbox-driven rack and pinion. The main source of movement is NEMA 17 stepper motor accompanied with a digital rotary encoder. Gear reduction of the gearbox is 1:562024. Rack and pinion do not affect gear reduction. With the gear reduction made, SPICAF is able to inject with a minimum resolution of 1 nl/hour (nanoliter) and a maximum resolution of 1 ml/hour (mililiter). This resolution is more than enough to qualify the spesifications by the WHO standars spesifications [14] which specifies the minimal flow rate range is 0.1 mL/hr.

The parameters and equation to calculate a formula and achieve injection succesfully is not specified in WHO standards. It is the developer's task to develop it. The formula to determine the required rpm for stepper motor to achieve the inputted flowrate is given below. Note that the user needs to input the flow rate in nL/hour. Since the formula finds rotation per minute, the nL/hour is converted to mL/minute first. The conversion from nL/hour to mL/minute is 1/60000000. To change the mL into into rotation, a ratio is needed based on the size of the syringe. Length of the syringe varies is ratioed with the stepper headgear size, in this case the headgear is 4,715 cm which is equal to 1 rotation of the headgear. Those are then applied to the formula:

$$rpm = \frac{flowrate * reduction\ gear\ ratio}{stepper\ rotation\ to\ syringe\ length\ ratio} * \frac{1}{6 * 10^7} \quad (1)$$

One full rotation of the NEMA 17 stepper motor in formula (1) is equal to 200 steps with 1.8° step angle, which is equal to 360° [18]. Since the stepper motor library works by setting the speed in step/s, we need to convert rpm into step/s using the formula below:

$$\frac{step}{s} = (rpm * \frac{200}{60}) \quad (2)$$

The injection subsystem features a soft starter implementation. The rotation speed of the stepper motor is measured using a digital rotary encoder. In addition to the rpm reading, the stepper motor performance was also measured when with and without an injection load until it reaches steady state. The experiment is run on 100 rpm, 200 rpm, and 300 rpm.

To determine the true accuracy of the instrument output, obtaining the actual output of the syringe and compare it to the entered data is necessary. However, it is difficult as there is no sensor capable of reading such small scale data for flowrate and volume. As a temporary solution, an alternative approach is to measure the stepper motor's rpm, provided that the gearbox and rack-pinion are ideal and computation . The expected outcome of the syringe injection process should be consistent with the stepper motor's rotation speed. Deductively, if the stepper motor is accurate, the injection process output is also accurate.

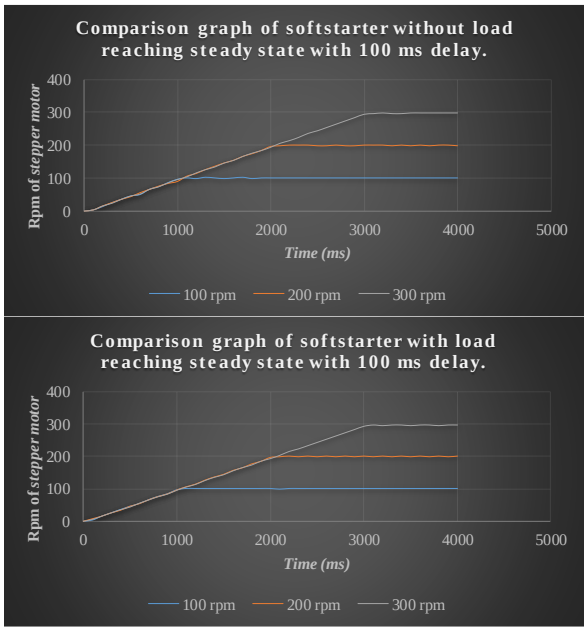

Fig. 5. Above: Graph of data measurement of the injection subsystem without load. Below: Graph of measurement data of the injection subsystem with the load

Measurements were made with a target rpm of 100 rpm (blue), 200 rpm (orange), and 300 rpm (green). The rpm reading by the encoder is obtained from the value of the phase *dt* (data)-pin to *clk* (clock)-pin [19] multiplied by two for each phase shift.

$$rpm = encoder * 2 \quad (3)$$

Both measurement graphs use a soft starter to reach a steady state. The soft starting feature works by repeatedly adding a constant from 0 to the desired rpm until it is attained. Additions are made every 100 ms. The results of the subsystem data indicate the time required to reach the target rpm and the significance of the load on the rpm speed of the stepper motor. The digital rotary encoder data for measuring rpm is accurate according to the specified input. The error that occurs is based on the limitations of the encoder, which misses reading of 0-3 rpm points from the actual rpm as described in the datasheet [19]. To get the accuracy of the injection, we calculate the percentage error of the reading, which is

$$Percentage\ error = \frac{|True\ value - Measured\ value|}{True\ value} * 100\% \quad (4)$$

The measured value of rpm after reaching steady state is often ±3 rpm of the actual value. Within 100 rpm to 300 rpm of inputs, the percentage error averages to ±2%. This formula from rpm reading to calculate accuracy is representative of the actual delivered liquid drug volume by the system with the rack and pinion part is considered ideal. According to WHO specifications [14], the volumetric flow rate accuracy with a common syringe should be ±5%. The SPICAF percentage error is ±2%, which passes the accuracy requirements.

The graph of the injection subsystem without and with load shows the presence or absence of injection does not affect the rpm of the stepper motor. The implementation of the soft starter also functions according to the intention where the stepper motor is run from 0 rpm to the target rpm. This implementation prevents stalling if the stepper motor directly runs at high rpm, because when the rpm is high, the torque produced by the stepper is low [20].

Soft starter time reaches steady state of 100 rpm in 1 second, 200 rpm in 2 seconds, and 300 rpm in 3 seconds. This is due to the addition of (+1) to the soft starter feature, which starts at 0 and has a delay of 100 ms each addition until the goal speed is reached. The given delay ensures that the encoder can read the soft starter rpm speed slowly and prevents current spikes from occurring in the A4988 driver when running the stepper motor. The time to reach steady state is not significant to the total operating time as the operating time usually runs in hours.

C. Interface Subsystem

The user interface subsystem interacts with the user via the keypad to receive input and the LCD to display the input. Each input, the LCD will refresh the screen to display the input. The number keys are used to enter numeric data, the C key to delete entries, and the D key to ENTER. Experiment limitations for this subsystem are the number keys and letter C and D. All output of the subsystem experiment is shown on the LCD.

Fig. 6. Top: Process of pressing keys on the keypad. Middle: Pressing the C key, the input is deleted and then ready to accept the new entry. Bottom: Receipt screen enters volumetric flowrate and enter numeric data

Volumetric flowrate entered in units of nL/hour. Based on the gear reduction of the injection propulsion subsystem, the minimum is 3600 nL/h and the maximum is 1080000 nL/h. Translated to motor rpm, the rotational speed reaches 1-300 rpm.

Based on the image of the test results, the subsystem was successfully operated according to its implementation objectives. The volumetric flowrate data entry only accepts numbers so that when the letters A, B, *, or # are pressed, they are not processed. The C button was successfully used to delete the input if the user entered incorrectly. The D key is successfully used to enter ENTER which will then be further processed by the system. Each time the button is pressed, the LCD successfully refreshes the screen to display the most recent input.

D. Notification Subsystem

The user notification subsystem plays a role in notifying users when a problem occurs. According to WHO specification standards, a minimum noise level of more than 45 dB (decibel) is required. SPICAF noise is generated by a passive buzzer. SPICAF notification noise was measured in decibels (dB) using the Android software Spectroid.

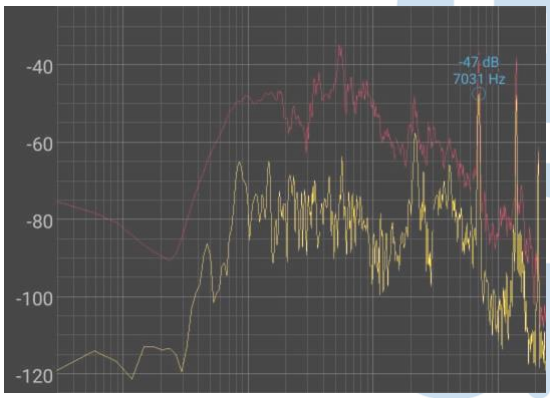

Fig. 7. Reading the buzzer noise using Spectroid

Noise measurements were taken at a 10 centimeter distance to mimic the user being near to the instrument. The noise measurement at an 8-meter distance depicts the user being outside of the room from the instrument. The experiment operates at a frequency range of 0 to 7500 Hz. Based on the limits stated above, the obtained data was shown in the graph below.

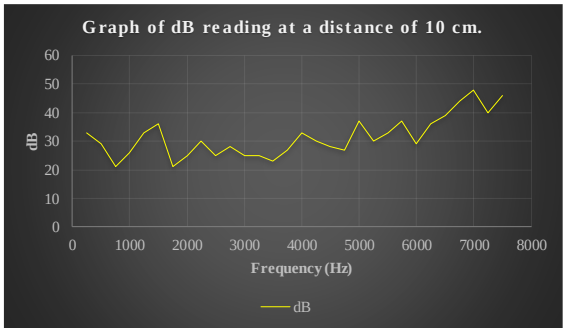

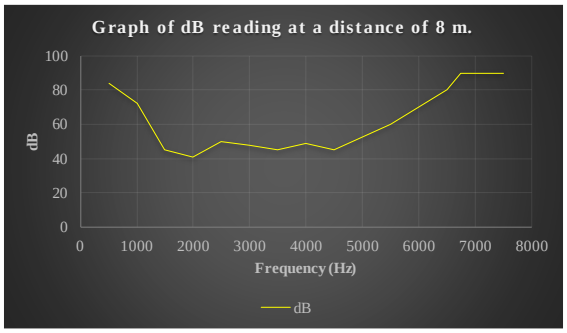

Fig. 8. Above: Buzzer noise measurements at a distance of 10 cm. Bottom: Buzzer noise measurements at a distance of 8 m

The graph of the data measurement shows the frequencies buzzer able to produce. The data read by Spectroid application shows that at distance of 10 cm, the buzzer reaches a noise of more than 45 dB after being more than equal to 7000 Hz (hertz), hence less than 7000 Hz noise produces less than 45 dB. For that, the buzzer will sound with a frequency of 7000 Hz.

For noise at a distance of 8 m, frequencies above 2000 Hz have reached more than 40 dB. When 7000 Hz the noise reaches 90 dB. At 1000-2000 Hz the noise is so disturbed by environmental noise that it becomes an outlier. Frequency of more than 2000 Hz is possibly affected by environmental noise.

E. Power Management Subsystem

The power manager subsystem (PMS) functions to supply power to the system. It ensures the system always have a backup power. The ATS transitions power from the adapter's AC (Alternating Current) source to the battery's DC (Direct Current) source when the AC power is not available [21]. The following pictures show the ATS operating conditions.

Fig. 9. Above: PMS state when using AC power adapter. Below: PMS state when using battery DC power

The truth table shows the PMS usage conditions when the AC adapter power is on, starting the battery usage and vice versa.

TABLE I. PMS TRUTH TABLE

ATS Truth Table	Adaptor	Battery
AC on	✓	×
AC off	×	✓

The truth table shows the PMS successfully delivered power between the AC adapter and the DC battery. When the AC power is off, the ATS pulls power from the battery. When AC power is available again, the ATS re-transitions the power to AC. Verification is done by checking the voltage on the adapter port MT36088 and battery port XL60099 when the AC condition is both available and inaccessible. This feature is partially achieved according to the intented specification following WHO standard [14].

The test results show, when making the transition, there is a delay. Delay arises from the use of relay logic, which is not an instantaneous operation. The delay that occurs causes the microcontroller to restart, losing it's operating process data before making the transition. Known temporary solution to this problem is to use a supercapacitor to fill the delay instantaneously, allowing the ATS to plug in the DC power from the battery without any delay. On the other hand, transitioning back from DC to AC is not problematic. It works as expected since the ATS can restore back it's AC power when it becomes available without losing any operational process data.

F. Data Logging Subsystem

The data logging subsystem functions to store data and enter it into the micro SD card via the micro SD card module. The form of the file created is a .txt because this type of file can be processed by the micro SD card module [22]. If the file is not on the micro SD card, the module will create it automatically [22]. The experiment began with a test run with submitted inputs. The data is subsequently stored to the micro SD card. After the operation, the micro SD card is unplugged and checked in a computer using a micro SD card reader.

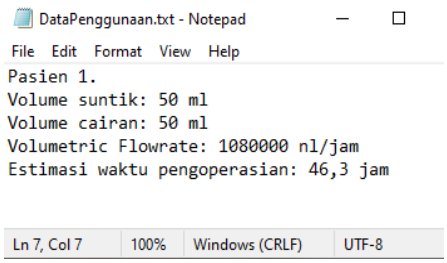

Fig. 10. A file named Usage Data stores the input data in .txt

The input data stored include the size of the injection volume used, the volume of drug liquid to be injected, the volumetric flow rate, and the estimated operating time of the injection, with the following formula:

$$Total\ time\ (hour) = \frac{Liquid\ volume\ (nl)}{Volumetric\ flowrate\ (\frac{nl}{hour})} \quad (5)$$

The standard injection sizes recommended by WHO are 20 cc, 50 cc, and 60 cc. The data logging subsystem successfully stores user input data that operates SPICAF. The micro SD card contains the DataUsage.txt file. The file contains data on the size of the injection, the volume of fluid entered, the input volumetric flow rate, and the estimated operating time obtained from the Total time calculation.

The data logging subsystem works by opening a file which is then filled in with data. After opening, the file must be closed again to end process for the file and ensure the module will save the data that has been inputted.

IV. CONCLUSION

Based on the results of testing and discussion, it can be concluded that the SPICAF system has been successfully built by WHO specifications and research feature targets. The bubble sensor subsystem successfully detects the air in the hose with the intensity of the light. The injection propulsion subsystem has succeeded in pushing the injection beyond the minimum specification with a soft starter implementation. The interface subsystem interacts with the user well. The notification subsystem can notify the user if an obstacle occurs with a specification of more than 45 dB. The data logging subsystem can store user input data.

The power manager subsystem can transition power from AC to DC and vice versa well, but for AC to DC, there is a delay so a supercapacitor is needed that can supply power instantly. In addition to the PMS solution, for future developments, a gear transmission method can be implemented in the gearbox to allow the working range of the SPICAF injection capability to be shifted. The fluid volume data is entered separately to allow the user to continue the rest of the drug that has not been injected or has failed. SPICAF can also be implemented with IoT (Internet of Things), such as data storage being saved directly to the user database, rather than stored in a micro SD card. For further development, it is necessary to do a real time test run of the injection process, since the accuracy measurement was performed using a different approach, which is reading it from the digital rotary encoder.

Since the development of SPICAF, the product has the specification capability to perform automatic data collecting, has backup power, can detect air through a bubble detector, can run a soft starter, has an alarm sound of more than 45 dB, and is capable of injection with a volume rate of 3600 nl. /hour up to 1080000 nl/hour.

ACKNOWLEDGEMENT

The author would like to thank Universitas Multimedia Nusantara for supporting this research.

REFERENCES

[1] Reynolds, R., Dennis, S., Hasan, I., Slewa, J., Chen, W., Tian, D., Bobba, S., & Zwar, N. (2018, January 9). A systematic review of chronic disease management interventions in primary care. *BMC Family Practice*, *19*(1). https://doi.org/10.1186/s12875-017-0692-3

[2] Shrestha, H., Bala, R., & Arora, S. (2014, May 19). Lipid-Based Drug Delivery Systems. *Journal of Pharmaceutics*, *2014*, 1–10. https://doi.org/10.1155/2014/801820

[3] Pardridge, W. M. (2012, August 29). Drug Transport across the Blood–Brain Barrier. Journal of Cerebral Blood Flow &Amp; Metabolism, 32(11), 1959–1972. https://doi.org/10.1038/jcbfm.2012.126

[4] U.S. Food & Drug Administration. (2018). *Infusion Pumps*. Available at: https://www.fda.gov/medical-devices/general-hospital-devices-and-supplies/infusion-pumps

[5] Jafarzadeh, M., & Farokhi, F. (2016, July). Design and construction of an automatic syringe injection pump. *Pacific Science Review A: Natural Science and Engineering*, *18*(2), 132–137. https://doi.org/10.1016/j.psra.2016.09.015

[6] Gorgich, E. A. C., Barfroshan, S., Ghoreishi, G., & Yaghoobi, M. (2015, December 18). Investigating the Causes of Medication Errors and Strategies to Prevention of Them from Nurses and Nursing Student Viewpoint. *Global Journal of Health Science*, *8*(8), 220. https://doi.org/10.5539/gjhs.v8n8p220

[7] Mirski, M., Lele, A., Fitzsimmons, L., Toung, T. K., & Warltier, D. (2007, January 1). Diagnosis and Treatment of Vascular Air Embolism. Anesthesiology, 106(1), 164–177. https://doi.org/10.1097/00000542-200701000-00026

[8] Malik, N., Claus, P. L., Illman, J. E., Kligerman, S. J., Moynagh, M. R., Levin, D. L., … Araoz, P. A. (2017). *Air embolism: diagnosis and management*. Future Cardiology, 13(4), 365–378. doi:10.2217/fca-2017-0015

[9] Hemauer, S. J., Kingeter, A. J., Han, X., Shotwell, M. S., Pandharipande, P. P., & Weavind, L. M. (2017, May). Daily Lowest Hemoglobin and Risk of Organ Dysfunctions in Critically Ill Patients. Critical Care Medicine, 45(5), e479–e484. https://doi.org/10.1097/ccm.0000000000002288

[10] Morrone, D., & Morrone, V. (2018). Acute Pulmonary Embolism: Focus on the Clinical Picture. *Korean Circulation Journal*, *48*(5), 365. https://doi.org/10.4070/kcj.2017.0314

[11] Flynn, F., Evanish, J. Q., Fernald, J. M., Hutchinson, D. E., & Lefaiver, C. (2016, August 1). Progressive Care Nurses Improving Patient Safety by Limiting Interruptions During Medication Administration. *Critical Care Nurse*, *36*(4), 19–35. https://doi.org/10.4037/ccn2016498

[12] Ahmed, M. G. A., Adam, A. B., Dennis, J. O., & Steele, G. S. (2009). Capacitor Device for Air Bubbles Monitoring. *International Journal of Electrical & Computer Sciences*, *9*(10), 93110–7878. https://doi.org/10.5281/zenodo.1056948

[13] Basjaruddin, N. C., Priyana, Y., & Kuspriyanto, K. (2013). Fault Tolerant Air Bubble Sensor using Triple Modular Redundancy Method. *TELKOMNIKA (Telecommunication Computing Electronics and Control)*, *11*(1), 71. https://doi.org/10.12928/telkomnika.v11i1.884

[14] World Health Organization. (2020). *COVID-19 Technical specifications for infusion devices*. WHO/2020-nCoV/MedDev/TS/InfDev. Available at: https://www.who.int/docs/default-source/medical-devices/tech-spec-infusion-devices-10072020-final-draft.pdf?sfvrsn=76f3e0fd_2

[15] Bolton, W. (2022, October 12). Mechatronics: Electronic Control Systems in Mechanical and Electrical Engineering (6th ed.). PEARSON INDIA.

[16] Musayev, E., & Karlik, S. E. (2003, December). A novel liquid level detection method and its implementation. Sensors and Actuators A: Physical, 109(1–2), 21–24. https://doi.org/10.1016/s0924-4247(03)00347-9

[17] ROHM Co. Ltd. (2014). *Digital 16bit Serial Output Type Ambient Light Sensor IC: BH1750*. https://components101.com/. Retrieved October 12, 2022, from https://components101.com/sites/default/files/component_datasheet/BH1750.pdf

[18] Changzhou Songyang Machinery & Electronics New Technic Institute. (2010, June 29). High Torque Hybrid Stepping Motor Specifications. Retrieved November 9, 2022, from https://components101.com/motors/nema17-stepper-motor

[19] Rotary Encoders. (2017). *Custom Raspberry Pi Interfaces*, 103–127. https://doi.org/10.1007/978-1-4842-2406-9_8

[20] Adafruit Industries. (2014, May 5). *All About Stepper Motors*. Adafruit Learning System. Retrieved October 13, 2022, from https://learn.adafruit.com/all-about-stepper-motors

[21] Alfariski, M. R., Dhandi, M., & Kiswantono, A. (2022, February 10). Automatic Transfer Switch (ATS) Using Arduino Uno, IoT-Based Relay and Monitoring. *JTECS : Jurnal Sistem Telekomunikasi Elektronika Sistem Kontrol Power Sistem Dan Komputer*, *2*(1), 1. https://doi.org/10.32503/jtecs.v2i1.2238

[22] Engineers, L. M. (2022, October 10). *Interfacing Micro SD Card Module with Arduino*. Last Minute Engineers. Retrieved October 12, 2022, from https://lastminuteengineers.com/arduino-micro-sd-card-module-tutorial/.

ISSN 2355-3286

Dynamic Ultrasonic Wave Generators as an Alternative Technology to Field Rat Repellents

Muhammad Jauhar Vikri[1], Roihatur Rokhmah[2]
[1] Information Systems, Universitas Nahdlatul Ulama Sunan Giri, Bojonegoro, Indonesia
[2]Computer Systems, Universitas Nahdlatul Ulama Sunan Giri, Bojonegoro, Indonesia
[1] vikri@unugiri.ac.id, [2]roiha.rohmah@unugiri.ac.id

Accepted 18 October 2022
Approved 30 November 2022

***Abstract*— The case of crop failure caused by pest attacks is one of the problems in agriculture that is always interesting to study. Apart from weather factors, pest attacks on rice and corn agricultural commodities often occur just before harvest time. Currently, farmers often use toxic materials and even electricity as a means to repel and eradicate rat pests. However, this method can be dangerous for the farmers themselves. There have even been several cases of death due to electrical equipment installed in agricultural areas. Based on these problems, a pest repellent will be made by utilizing ultrasonic waves from a solar-powered power source so that it can be used efficiently, practically and safely. This tool is built using IC NE556C, Solar Panel, LDR Sensor (Light Dependent Resistor), and Ultrasonic Piezo PTC 4000 Speaker. IC NE556C timer and ultrasonic wave multivibrator are used to generate ultrasonic waves randomly according to the program. The purpose of making this tool is as an alternative to field mouse pest repellent using ultrasonic waves by utilizing solar energy in handling pests in agricultural areas.**

***Index Terms*— agriculture; rat pests; solar energy; ultrasonic waves.**

I. INTRODUCTION

The agricultural sector in Indonesia still plays a very important role for the country. Success in the agricultural sector will contribute significantly. However, this success is often hampered by the presence of rice field rats (*Rattus argentiventer*) [1]. Rice field rats are pests of various gardens, especially rice plants. This pest often results in crop failure for farmers.

Sectors in several regions in Indonesia often fail due to changes in natural conditions including climate, wind and temperature changes as well as several other factors, namely viruses, fungi, insect pests and rodents in excess on agricultural land [2]. Rice field rats are the main pests of rice plants from the mammal class which have very different characteristics compared to other types of rice pests. Rice field rats damage rice plants at all stages of rice plant growth and in rice storage warehouses. Severe damage occurs if the rats attack the generative phase, because at that phase the plant does not have the ability to form new tillers [3]. Rats damage rice plants starting from the center of the plot, then extending towards the edges [4]. Rats attack rice at night, during the day rats in holes in irrigation embankments, rice fields and village areas near rice fields. In the fallow period (the period before tillage) most of the rats migrated to the village area near the rice fields and returned to the rice fields after the rice crop was approaching its phase. Rice field pests are not only rats, but birds are also one of the rice field pests that can harm farmers [5]. Rice is one type of grain that is high in protein that is favored by birds [6]. No wonder the rice field birds attack the rice starting to turn yellow.

A large increase in the population of rice field rats recently occurred in Bojonegoro Regency, East Java province, which resulted in damage to rice and corn plants which resulted in crop failure. Control of rat pests is currently carried out in the traditional way by finding rat nests and catching these mice, the Javanese call them "*gropyokan"*, pumping water into the rat's nest and electricity [7]. The research that will be carried out utilizes the technology of using ultrasonic waves to repel rice field rats and so it is hoped that it will help farmers, especially farmer groups in Sugihwaras District, Bojonegoro Regency in dealing with rat pests. In addition, it will analyze several methods of rat repellent that have been carried out so that the most effective, inexpensive and safe method of rat repellent will be obtained.

The novelty in the application of solar energy rice field mouse pest repellent is the simplicity of the device circuit but the ultrasonic wave output can be programmed by detecting the brightness of the light with a light sensor to detect day and night. The ultrasonic waves produced can be set statically or swing dynamically simultaneously, so by applying this pattern the device can effectively repel pests by disrupting passive feeding behavior patterns and passive motion of pests.

In 2018, Azharul conducted research on farmers' rice fields with an area of about 200 ha with the aim of studying the breeding characteristics of paddy rats as a basis for control [8]. Observations included reproductive conditions, pregnancy, number of children, number of embryos, and number of placental scars. The results showed that the breeding of paddy rats in rice plants mainly occurred in the rice generative stadia period. In one growing season there were three births of rats with an average of 10 cubs for each birth. The highest number of children occurred in the first birth and decreased in subsequent births. The breeding ground for rice rats is mainly in the habitat of irrigation embankments. Based on the breeding characteristics, the control of the rice field rat population should be carried out early (early planting) before the rats breed, with the main target of controlling the irrigated embankment habitat. Application of pattern and timing of rice planting simultaneously can limit the breeding of field rats. This research is used as scientific information about rice field rats breeding for the proposed research.

In 2019, Oktivira conducted a study to determine the effect of crickets' ultrasonic waves on passive feeding behavior patterns and passive motion of rats [9]. Ultrasonic waves of crickets were exposed directly to rice field rats and observed through passive feeding behavior patterns and passive motion of rats were analyzed by factorial design variance. The observed factors include frequency, source distance, and duration of exposure to ultrasonic waves of crickets and their combination. The frequency of ultrasonic waves of crickets at a distance of 100 cm and a length of exposure of 45-60 minutes can cause changes in passive feeding behavior and passive motion of rats. This research by Tito adds to the reference that ultrasonic waves of crickets are able to influence the behavior of field rats[10].

In 2020, Fatahullah researched the application of pest control using the Arduino microcontroller[11]. With a focus as an appropriate technology, researchers utilize a microcontroller device with a solar power source as the main energy of the device [12], [13]. However, in this device, the light sensor device functions as a switch to turn off the device at night.

In 2020, Hikmah researched the use of a prototype bird repellent using a motion sensor to activate ultrasonic waves according to the detected bird target [14], [15]. The purpose of this research is to design and build a prototype of field mouse pest repellent in rice fields based on the internet of things (IOT). The focus is on sparrows, with the use of ultrasonic speakers with a certain frequency to repel leafhoppers and rats. This prototype is connected to the internet network which can be monitored and controlled remotely using desktop and android. Based on the results of the analysis in this study as input using the RCWL Microwave motion sensor [16]. able to repel pests by targeting rats and birds.

In 2022, Devika et al made a study using ultrasonic sound waves to disturb birds passing through the field. hardware and software used in this research are camera, object detection, buzzer, Arduino, OpenCV, and pySerial. This study used a video stream by utilizing YOLOv3 to detect birds crossing the area. When a bird crosses the area and is detected by the object detection video, the buzzer alarm will sound to turn on the ultrasonic sound wave so that the bird will be disturbed and leave the area [17].

The novelty in the proposed research, is the method of applying ultrasonic wave generation technology with a solar energy source to repel pests in rice fields having a novelty in incorporating the resulting ultrasonic wave output. which combines static and dynamic ultrasonic waves at the same time. If in previous studies using ultrasonic waves which are only emitted in a certain frequency range, this device is expected to combine static ultrasonic waves from the first speaker and dynamic ultrasonic waves from the second speaker. In addition to the simplicity of the design, what is superior in this device this novelty will be an interesting thing to learn.

Rats are agricultural pests that are quite skilled at adapting to new environments [18]. Based on the literature study, it is necessary to make better adjustments to the device to deal with this problem. So, it is necessary to add the innovation of combining the static and dynamic output of ultrasonic wave frequencies.

This device is designed without using a microcontroller programming, but even so the device will be able to effectively work to emit ultrasonic waves properly. By applying a light sensor or Light Dependent Resistor (LDR) for day or night detection, the device will generate ultrasonic waves according to predetermined settings according to pest behavior during the day and night. Besides the waves can be adjusted statically, the ultrasonic waves generated can swing like a dynamic whistle method so it will be difficult for pests to adapt.

II. METHOD

The research method used in this study is described as follows. Initially, a literature study was carried out to determine the basis for research and design alternative technology for field mouse pest repellent using ultrasonic waves with solar power supporting devices and light sensors, so that they can implement and find the supporting theory needed to provide the basis used for this research. A study was then conducted to find out whether this system was feasible to be developed or not, including to review the benefits resulting from the application of the system to be designed and developed. Among the various available

methods, the prototyping method was chosen to design and develop Ultrasonic Wave Generators as Alternative Pest Repellent Technology.

A. Literature Study Method

Studying the results of research that has been published in research journals on the use of ultrasonic waves and the behavior of field rats.

B. Field Study Method

Directly observing the behavior of rats on agricultural land in Sugihwaras Village, Sugihwaras District, Bojonegoro Regency.

Conducted a discussion with the Women's Farmer's Group in Sugihwaras Village, Sugihwaras Subdistrict, Bojonegoro Regency about the methods of getting rid of field rats that have been carried out in the area. So that it can provide counseling about the method of field rat repellent in the scope of electrical safety. Before providing counseling, an analysis of the field mouse pest repellent method that has been carried out and provides an alternative new method using ultrasonic waves in order to obtain an efficient, inexpensive and safe method of field mouse pest repellent.

C. Data Analysis Method

Conducted an analysis of several methods of rat repellent, both conventional and with the use of ultrasonic wave generators.

D. Conclusion Method

Conclusions were obtained based on the results of field studies and data analysis to obtain a safe, effective and inexpensive method of rat repellent.

E. Research Variable

The research variable in question is everything that will be the object of research. Variables can also be interpreted as factors that play an important role in this study, namely making a series of ultrasonic wave generators with a certain voltage and frequency that can disrupt the behavior of rice field rats so as not to damage rice plants, as well as observing the distance range when ultrasonic waves can disrupt the behavior of rice field rats. directly applied to paddy fields.

III. RESULT AND ANALYSIS

A. The Flowchart

To provide an overview of how the system functions, the following figure depicts the flowchart of the developed systems (Fig. 1). in the flowchart shown in Fig.1, the light sensor will only detect day and night. if the sensor has recognized the intensity of the light detected, the electronic circuit will emit an ultrasonic sound according to the settings that have been set using a potentiometer.

Potentiometer component is used to set the ultrasonic wave output. on the first potentiometer, serves to adjust the ultrasonic wave with a stable output, simultaneously the device will issue a fixed ultrasonic sound wave. then on the second potentiometer, serves to adjust the ultrasonic wave with a random output at a certain frequency range. This is done so that the rats have difficulty adapting to a fixed wave. In the novelty of the combination of the fixed and random wave method, it is hoped that it will be more effective in creating a rats repellent device.

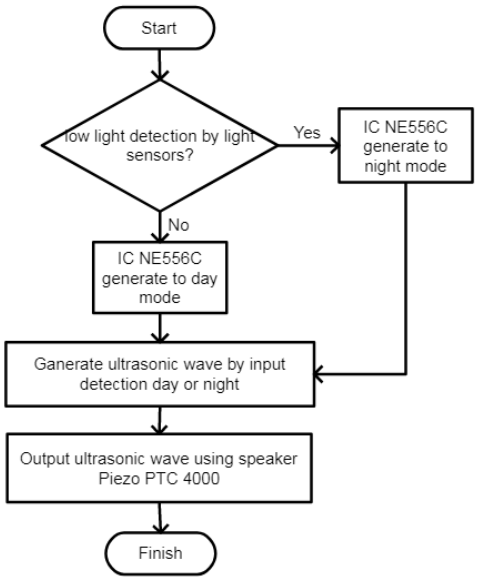

Fig. 1. System Flowchart

From the flowchart, it can be seen that the light sensor plays a role in detecting day and night, how to detect day and night obtained from bright lighting will be detected as day and less lighting will be detected as night. if it has been detected day and night, the IC NE556C will generate ultrasonic waves. it is intended to set day mode and night mode on the device manually. the result of the settings that have been made, the system will automatically emit ultrasonic waves according to day and night modes for the purpose of disturbing rat pests.

B. The System Design

The general mechanism of Solar Cell Energy and Light Sensors in Ultrasonic Wave Generators as Alternative Pest Repellent Technology is illustrated in the Figure 2.

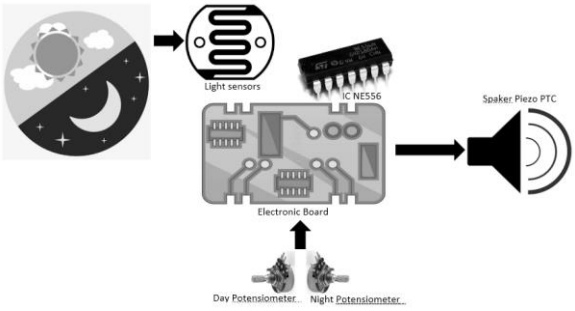

Fig. 2. General System

The following is an explanation of how to start system implementation the use of Solar Cell Energy and Light Sensors in Ultrasonic Wave Generators as Alternative Pest Repellent Technology:

1. LDR Sensor (Light Dependent Resistor), it will detect the intensity of light entering the system. if the light intensity is low, it will be detected as night and if the light intensity is high, it will be detected as day [19].
2. The manual setting using day and night potentiometers to provide different frequencies during day and night. the goal is that rice field rats (*Rattus argentiventer*) difficult to adapt to the ultrasonic sound produced [20].
3. The IC NE556 component will generate the resulting ultrasonic waves by swinging the predetermined ultrasonic wave range [17].
4. In the experiment the use of solar cell energy and light sensors in ultrasonic wave generators as alternative pest repellent technology, the experiment will be carried out by testing rat pests by providing various ranges of ultrasonic waves. The test will observe how much the rat will respond to the ultrasonic waves that have been generated by the electronic device.
5. The purpose of giving ultrasonic waves to rats is so that the rats are disturbed and will eventually respond to avoid the waves. this will prove that the rats repellent device is functioning properly.
6. The output of this device will combine different ultrasonic wave outs, namely the ultrasonic wave frequency that is fixed and dynamic with the aim that the rice field rats are not able to adapt.

The general digital circuit for solar cell energy and light sensors in ultrasonic wave generators as an alternative to field mouse pest repellent' technology is illustrated in Figure 3. In this digital circuit, the NE556 Integrated Circuit as the main component of the digital circuit was chosen because from various previous tests the NE556 IC proved better in producing ultrasonic waves and have more durability.

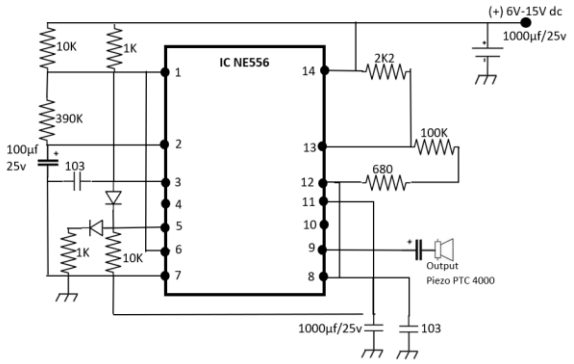

Fig. 3. General digital circuit for Solar Cell Energy and Light Sensors in Ultrasonic Wave Generators as Alternative Pest Repellent Technology

The IC NE556 series will activate ultrasonic waves with a certain range based on the settings with the potentiometer [21]. There are 4 modes of setting the ultrasonic waves generated (Fig. 4):

1. Frequency modes are the 45-48 MHz frequency mode in V_2 mode and 45 MHz constant in V_1 mode.
2. Frequency modes are above 40-45MHz in V_2 mode and constant 40 MHz in V_1 mode.
3. Frequency modes are above 35-40 MHz in V_2 mode and 35 MHz constant in V_1 mode.
4. Frequency modes are above 35-40 MHz in V_2 mode and constant 35 MHz in V_1 mode.

So that the frequency mode can be activated during the day and night as a dual timer [22]. So that each day and night mode can be set with variations of the four ultrasonic frequency modes.

Fig. 4. The IC NE556 display

C. *System Implementation*

The experimental scenario consists of 2 main scenarios, namely experiments with a static frequency and with a swing frequency or swinging a specified frequency range. In the first scenario, the experiment will be carried out using a method of providing a static or fixed frequency with a certain time span, while in the second scenario, it will be carried out by a method of providing dynamic or swing frequencies with a certain time span.

At the time of testing the device, the device is placed in a rice field area with a height of 40 cm from the ground (Fig. 5). Previously the agricultural area had

been selected with flood-free conditions and not affected by pests and during the vegetative plant period. The vegetative period was chosen because at this time, rats began to attack rice plants.

Fig. 5. The device implemented in the fields

1) First Experiment

The first experimental scenario, the pattern and behavior of rats were tested with a rat repellent device with various levels of frequency with a certain time span. By using a spectrum analyzer device [23], ultrasonic frequencies are detected in real conditions according to the environment. The picture shows the active ultrasonic spectrum in the 48 kHz range. In the research experiment, the rats used in the experiment were field rats (*Rattus argentiventer*) which are the main pests of rice plants. The experiment was carried out by placing mice in the same room simultaneously and observing the behavior of the mice during the experiment.

TABLE I. FIRST EXPERIMENT

No	Frequency (kHz)	The number of Rats to									
		1	*2*	*3*	*4*	*5*	*6*	*7*	*8*	*9*	*10*
1	20	0	0	0	0	0	0	0	0	0	0
2	25	0	0	0	0	0	0	0	0	0	0
3	30	0	0	0	0	0	0	0	0	0	0
4	35	0	0	0	0	0	0	0	0	0	0
5	40	0	1	0	0	1	0	0	1	0	1
6	41	1	1	1	1	0	1	1	0	1	0
7	42	1	1	1	1	1	1	1	1	1	0
8	43	1	0	1	0	1	1	1	1	1	1
9	45	1	1	1	1	1	1	0	1	1	1
10	46	1	1	1	0	1	1	1	1	1	1
11	47	1	1	1	1	1	1	1	1	1	1
12	48	1	1	1	1	1	1	1	1	1	1

The first experiment, a summary of the experimental results is shown in Table I, there are two reactions of rats which are recorded by giving the number symbols 0 and 1. a reaction that shows the number 0 means that the mouse does not respond to ultrasonic sound and a reaction that shows the number 1 means that the mouse responds to sound ultrasonic.

2) Second Experiment

In the second experimental scenario, the pattern and behavior of the rats were tested with a rat repellent device with various levels of frequency with a certain time span. In the second experiment, the tool will be set to swing mode or the frequency of swinging up and down with a predetermined frequency range.

TABLE II. SECOND EXPERIMENT

No	Frequency (kHz)	The number of Rats to									
		1	*2*	*3*	*4*	*5*	*6*	*7*	*8*	*9*	*10*
1	20-30	0	0	0	0	0	0	0	0	0	0
2	25-35	0	0	0	0	0	0	0	0	0	0
3	30-40	0	0	1	1	1	0	1	1	1	0
4	35-45	0	1	1	1	1	1	1	1	1	0
5	40-45	1	1	1	1	1	1	1	1	1	1
6	42-48	1	1	1	1	1	1	1	1	1	1

In Table 2, rats were given ultrasonic waves with various frequency ranges from 20 kHz to 48 kHz. But in the second experiment, ultrasonic waves will use the swing method such as the whistling concept.

After doing several ultrasonic waves testing on rats, the table shows a summary that describes each condition of the rats to ultrasonic waves. In the summary of the behavior of this ultrasonic wave, it will be a constant reference for ultrasonic waves to disturb rice rats.

a) Summary at 30 kHz

TABLE III. EXPERIMENT RESULT SUMMARY 30 KHZ

Repetition	Frequency (kHz)	Behavior
1	30	affected, respond
2	30	affected, respond
3	30	affected, respond

In Table 3, for testing the ultrasonic frequency of 30 kHz, the field rat pest began to respond to the arrival of the disturbed ultrasonic sound source but its behavior was still said to be not so disturbed. they still tolerate the sound that comes out.

b) Summary at 35 kHz

TABLE IV. EXPERIMENT RESULT SUMMARY 35 KHZ

Repetition	Frequency (kHz)	Behavior
1	35	affected, respond
2	35	affected, respond
3	35	affected, respond

In Table 4, for testing the ultrasonic frequency of 35 kHz, rice field rats respond to the arrival of the ultrasonic sound source and are disturbed but their behavior is still said to be not so disturbed. they still tolerate the sound that comes out.

c) Summary at 40 kHz

TABLE V. EXPERIMENT RESULT SUMMARY 40 KHZ

Repetition	Frequency (kHz)	Behavior
1	40	away from the sound source
2	40	away from the sound source
3	40	away from the sound source

In Table 5. for the 40 kHz ultrasonic frequency test, the rice field rat pest began to be disturbed but from its behavior it was still said to be not so disturbed, when the frequency was greater than 40 kHz i.e. 40.5 kHz the behavior of the rat began to be very disturbed, the rat was confused looking for a gap to get out. from his cage.

d) Summary at 45 kHz and higher

TABLE VI. EXPERIMENT RESULT SUMMARY 45 KHZ

Repetition	Frequency (kHz)	Behavior
1	45	away from the sound source
2	45	away from the sound source
3	45	away from the sound source

In Table 6. for testing ultrasonic frequencies above the 45 kHz to 48 kHz waves. in the frequency range of 45 kHz to 48 kHz the rats began to be very disturbed; the rats were confused looking for a gap to get out of their cage. It's a good thing that this study succeeded in getting the rats away from the source of the sound.

IV. CONCLUSION

In the experiment of rat behavior on ultrasonic waves concluded that the average rat responds to ultrasonic waves. The response shown is that the rat avoids the sound source. The affective ultrasonic sound waves in the use of this tool are in the range of 40 kHz to 48 kHz. Testing of equipment with frequencies above 50 kHz has not been carried out because of the capabilities of the equipment at the 50 kHz limit. So, with this matter the test limit is carried out below 50 kHz with consideration of the level of resistance of the PIEZO CT 4000 tool as ultrasonic sound output.

The device's power supply requires a voltage of 12V 10A using a lithium type battery [24]. The device has been tested to be able to meet the electrical power of the device overnight or without sunlight for more than 12 hours. The light sensor on the device will activate day and night modes according to the intensity of the light entering the sensor. Measurement of sound range in open area with Infrasound Detector, can be detected at a distance of 75 meters.

From various tests and experiments conducted, research shows that, ultrasonic wave testing on white rats shows effective results in the frequency range of 40.5 up to 48 kHz, with the average reaction away from the wave source (speaker) and moving aggressively. This shows that the white rat's sense of hearing will be disturbed in the ultrasonic wave capacitor range of 40.5 up to 48 kHz.

ACKNOWLEDGEMENT

We thank the Ministry of Research, Technology and Higher Education DRPM for funding this research. This is a research conducted under the Beginner Lecturer Research Grant scheme for the 2022 Fiscal Year.

REFERENCES

[1] D. L. Pakiding dan A. Tahendrika, "Motivation Analysis Of Farmers Still Maintaining The Processing Of Unproductive Rice Farming Land From A Local Cultural Perspective," JManagER, vol. 1, no. 2, pp. 12–23, 2022.

[2] A. Ansari, Y.-P. Lin, dan H.-S. Lur, "Evaluating and adapting climate change impacts on rice production in Indonesia: A case study of the Keduang Subwatershed, Central Java," Environments, vol. 8, no. 11, pp. 117, 2021.

[3] T. Xuan, T. Yen, dan T. Caugh, "Understanding Farmer and Government Measure in Rat Pests Control in Rice Fields," Journal La Lifesci, vol. 2, no. 2, pp. 24–30, 2021.

[4] A. Najih, H. Kuswanto, Y. P. Rahmat, dan A. N. Cahyani, "The effect of frequency owl's sound, crickets, and combination of both towards rat reaction," dalam AIP Conference Proceedings, 2019, vol. 2202, no. 1, pp. 020009.

[5] K. D. Nurikhsani dan J. Mupita, "Benefits and Effectiveness of Automatic Farmer Pest Repellent," ASEAN Journal of Science and Engineering, vol. 2, no. 3, pp. 243–248, 2021.

[6] B. C. Debnath dan T. K. Das, "Nutrient Requirements of Ducks And Their Feeding," dalam Duck Production and Management, CRC Press, pp. 17–47.

[7] M. Cimorelli dkk., "A voltage-sensitive ultrasound enhancing agent for myocardial perfusion imaging in a rat model," Ultrasound in Medicine & Biology, vol. 46, no. 9, pp. 2388–2399, 2020.

[8] Q. Azharul dan A. U, "*Rancang Bangun Alat Monitoring Pergerakan Objek pada Ruangan Menggunakan* Modul RCWL 0516," J. Tek. Elektro, vol. 10, pp. 41–46, 2018.

[9] O. N dan Kholis, "*Prototype Sistem Pengusir Hama Burung Dengan Catu Daya Hybrid Berbasis IOT*," J. Tek. Elektro, vol. 9, pp. 735–741, 2019.

[10] S. I. Tito, B. Yanuwiadi, dan C. Sulistya, "*Pengaruh Gelombang Ultrasonik Jangkrik (Acheta domesticus) terhadap Pola Perilaku Makan Pasif dan Gerak Pasif Tikus Sawah (Rattus argentiventer)*," J-Pal, vol. 1, no. 2, pp. 80–94, 2011.

[11] Fatahullah (Universitas Muhammadiyah Makasar), R. (Universitas M. Makasar), dan J. (Universitas M. M. H, "*Perakus (Pengendali Hama Serangga Dan Tikus) Alat Tepat Guna Otomatis Berbasis Mikrokontroler Sebagai Solusi Pangan Tanpa Pestisida Kimia*," *Penelitian dan Penalaran*, vol. 7, no. 1, pp. 53, 2020.

[12] H. A, "*Rancang Bangun Alat Pengusir Hama Tanaman Menggunakan Gelombang Ultrasonik Dengan Variasi Letak Dan Jumlah Sumber Gelombang*," Politeknik Ati Makassar, 2018.

[13] M. M. Shahjalal, M. Manna Mehedy, M. Mijanur Rahman, M. Tuhin Ali, dan A. H. Bagdadee, "Using microcontroller based solar power system for reliable power supply," Journal of Applied and Advanced Research, vol. 7, pp. 18–24, 2022.

[14] N. Hikmah dan A. Khumaidi, "*Rancang Bangun Prototipe Pengusir Hama Burung Menggunakan Sensor Gerak Rcwl Microwave Berbasis* Internet Of Things," Simetris, vol. 11, no. Internet Of Things, pp. 2, 2020.

[15] N. Hema, "Solar powered Smart Ultrasonic Rodent Repellent with DTMF and Manual Control for Poultry farms," International Journal of Progressive Research in Science and Engineering, vol. 3, no. 04, pp. 115–120, 2022.

[16] M. Alhan, Y. Finayani, A. Haryawan, dan M. H. Hanafi, "Pengusir Hama Tikus Sawah Berbasis Gelombang Ultrasonik," vol. 20, no. 1, 2021.

[17] D. Sunil, R. Arjun, A. Ashokan, F. Zakir, dan N. P. John, "Smart Crop Protection System from Birds Using Deep Learning," dalam Emerging Technologies in Data Mining and Information Security, Springer, 2021, pp. 621–632.

[18] G. Govinda Raj, "Rodents," dalam Pests and Their Management, Springer, 2018, hlm. 973–1013.

[19] A. B. Balogun, S. A. Adebanji, dan U.-O. Idiong, "Energy Efficient Automatic Walkway Lighting System Using A Light Dependent Resistor," pp. 12, 2022.

[20] A. Khan, M. A. Ashraf, M. A. Javeed, M. S. Sarfraz, A. Ullah, dan M. M. A. Khan, "Electronic Guidance Cane for Users Having Partial Vision Loss Disability," Wireless Communications and Mobile Computing, vol. 2021, pp. 1–15, Okt 2021, doi: 10.1155/2021/1628996.

[21] B. Ulmann, Analog Computing. Walter de Gruyter GmbH & Co KG, 2022.

[22] V. Kumar dan S. Kumar Raghuwanshi, "Hardware Implementation of Prepaid Power Consumption Using Coin Box System," IOP Conf. Ser.: Mater. Sci. Eng., vol. 1116, no. 1, Apr 2021, doi: 10.1088/1757-899X/1116/1/012177.

[23] Y. Zhyvaha, H. Klym, dan R. Dunets, "Cost Efficient Audio Spectrum Analyzer: Design and Study," dalam 2021 11th IEEE International Conference on Intelligent Data Acquisition and Advanced Computing Systems: Technology and Applications (IDAACS), 2021, vol. 1, pp. 432–437.

[24] N. K. Raghavendra dan K. Padmavathi, "Solar charge controller for Lithium-Ion battery," dalam 2018 IEEE International Conference on Power Electronics, Drives and Energy Systems (PEDES), 2018, pp. 1–5.

ISSN 2355-3286

An Analysis Of The Performance Of Autonomous Navigation On An Ardupilot-Controlled Rover

Adik Susilo Wardoyo[1], Indri Purwita Sary[2], Ilham Taufik Maulana[3]
[1] Prodi Teknik Elektronika, Politeknik Gajah Tunggal, Tangerang, Banten, Indonesia
[2] Prodi S1 Teknik Elektro, Fakultas Teknik , Universitas Singaperbangsa, Karawang, Jawa Barat, Indonesia
[3] Prodi Teknik Mesin, Politeknik Gajah Tunggal, Tangerang, Banten, Indonesia
[1] adiksusilo@poltek-gt.ac.id, [2] indripurwitasary@gmail.com, [3] ilham@poltek-gt.ac.id

Accepted 25 October 2022
Approved 23 November 2022

***Abstract*— Monitoring forests is one of the strategies in the overall preventive strategy. Monitoring the forest can quickly and permanently manage how tree illnesses emerge, spread, and evolve. To help monitor forest fires, a robot platform that can operate independently and assist in data collection can be created. In this paper, the accuracy of the Ardupilot-controlled autonomous navigation system of the rover was examined. The metode are used is experimental study, the study consists of a comparison between the GPS rover log and the SITL simulation within the mission planner tool. The average accuracy achieved by altering the route's distance and shape is 94.58%. The lengthy path may be the source of the rover's inaccurate autonomous navigation. In this case, the turning angle problem has no real effect on how well and accurately the rover navigates on its own.**

***Index Terms*— Ardupilot, Autonomous, GPS, Navigation, Rover.**

I. INTRODUCTION

A. Robot for Forest Fire Monitoring

Monitoring forests is one of the strategies in the overall preventive strategy since it is crucial to stopping the spread of tree diseases and forest fires. In addition to determining the general health of the forest, monitoring the forest can quickly and permanently manage how tree illnesses emerge, spread, and evolve. On the other hand, pathologists who research forests usually discover that they cannot visit many distant areas of the forest within a reasonable length of time or at a reasonable cost. To help monitor forest fires, a robot platform that can operate independently and assist in data collection in the forest can be created [1]. In their paper, Khaled et al. have already conducted a simulation to investigate the effectiveness of their proposed algorithm using teams of unmanned ground vehicles (UAV and Unmanned Ground Vehicles (UGV) for fire detection in the forest [2]. Merino et al. have previously produced a study that demonstrates it is possible to construct unmanned aircraft systems (UAS) for detecting forest fires. Experiments have shown that systems based on airplanes can be highly helpful for firefighting tasks such as fire monitoring. This is because aircraft systems can bridge the gap between the geographical scales provided by systems based on satellites and those based on cameras on towers. The UAS is able to modify its deployment such that it sidesteps the drawbacks of traditional methods, such as the presence of smoke, or covers areas that are more conveniently located [3]. Quenzel et al. already make robots capable of doing their assigned jobs on their own, and their vision, motion planning, and fire extinguishing systems are reliable [4]. Based on some of the references above, it can be concluded that the use of autonomous robots can be carried out for monitoring, one of which is forest fires.

B. Mobile Robot

A wheeled autonomous robot is one of the existing robot types. A wheeled robot system can be created by combining several electronic and mechanical components. As an autonomous controlling device, a guiding component can be added to the robot's navigation. Typically, the control function uses GPS as a position reference, but other guiding components, such as cameras, radars, and others, can also be added. Mobile robots are robots that can travel from one location to another to do required and difficult activities, simple jobs that are time-consuming, repetitive, or dangerous. These days, people are being replaced by robots in a variety of settings, including offices, the military, medical operations, sports, agricultural tasks, and many more. Mobile robots can be built in a variety of ways, but thanks to the recent proliferation of embedded systems and microcomputers, it is now feasible to create low-cost solutions. Mobile robots come in a variety of shapes and sizes [5].

Mobile robots can have a variety of configurations, a variety of sensors (infrared, ultrasonic, webcams, GPS, magnetic, etc.), and a variety of command and control algorithms, depending on where they are going.

Mobile robots can also be supervised either locally or remotely [6]. Ananta et al. in their research have already built their autonomous rover controlled by Ardupilot, and the result of accuracy is about 89,43% [7]. Rahim et al., who have succeeded in designing a lawnmower that works autonomously using an Ardupilot made to cut weeds [8]. Hassan and his team were able to design a Robot Unmanned Ground Vehicle that can follow and move waypoints sent from the ground station by using the Ardupilot APM 2.6 controller and the Mission Planner program [9].

C. *Ardupilot and APM*

The firmware for the autonomous unmanned system is typically developed with the help of ArduPilot, which is a very common framework [10]. Ardupilot is an open source navigation software that allows the development of reliable autonomous unmanned vehicle systems, e.g. for multirotor drones, fixed-wing and VTOL aircraft, helicopters, ground rovers, ships, submarines, and tracking antennas. To support the use of Ardupilot, the mission planner application can be used as an interface with the controller to set up, configure, test, and tune the vehicle. Mission planner is a Ground Control System (GCS) application that has full features and is compatible with Ardupilot [11]. According to the findings of Carlson's investigation, one of the most popular open-source platforms for drones is called Ardupilot. This platform is compatible with a variety of hardware and software options. Some examples of hardware that is compatible include the Pixhawk line, the Ardupilot Mega, etc. There is compatible software such as Mission Planner, APM Planner, and QGroundControl, etc. [12].

D. *Ardupilot Analysis*

In a study carried out by Liu et al., it was revealed that when comparing the simulated SIL and the experimental performance of the Ardupilot controller on UAV, a promising result was obtained [13]. In their experiment, Janarthanan et al. get the result that the Ardupilot APM 2.8 is capable of controlling the UAV by path planning with an 82 % success rate from 3 trials [14]. Jung and Ariyur's research already tests and improves the GPS performance of the Unmanned Ground Vehicle (UGV) controller by Ardupilot APM 2.6 [15]. In their research, Timpitak et al. have succeeded in comparing simulations of autonomous navigation systems using the Matlab simulink program and experiments, with good results in heading to the target position autonomously. The experiment was carried out with the coordinates of the GPS logger in the robot, compared with the simulation, then from these results the error difference was sought [16]. This research will be conducted by testing the performance of the rover's navigation system in light of these investigations. Rover will be controlled using Ardupilot APM 2.8 while Mission Planner will serve as the base station application. GPS log data from the simulation will be compared to data from the experiment.

II. METHOD

A. *Hardware Configuration*

The method used is an experimental study that consists of a comparison between the GPS rover log and the SITL simulation within the mission planner tool. The GPS logs analyzed in the study are GPS log data from simulations and GPS logs for robot rovers. The rover is assembled using the chassis of a modified remote control car, as the rover controller uses Ardupilot Mega 2.8, the GPS module uses the M8N GPS module, and 1 servo and 1 ESC as controller and driver. An 11.1 volt, 5000 mAh battery is used to power the robot. The XBee Pro 900HP wireless module, with a working frequency of 2.4 GHz, is used to connect the Ardupilot telemetry system to the base station, The schematic and the assembled rover are shown in Fig 1.

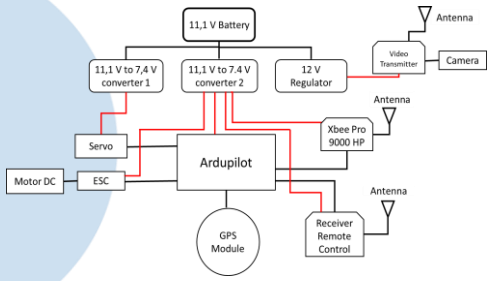

(a)

(b)

Fig. 1. (a) Rover Schematic, (b) Rover with Ardupilot controller

The data from the rover is then sent in real time to the base station, using the Xbee module as the transmission medium. The data is then displayed and saved via the Mission Planner application. In addition, through this application, it can be used to program the rover parameters and program the route to be traversed by the rover. Apart from being in auto mode, the rover also has a manual mode in which the control of the rover can be controlled manually via the Flysky FS I6 remote control with a 6 channel FS i6B receiver. The robot also has a camera and a transmitter system. The video is sent to the receiver, where it will be shown and

saved in the Mission Planner application. The rover system and base station application are depicted in Fig 2.

Fig. 2. (a) Rover Schematic, (b) Rover with Ardupilot controller

B. *Data Collection and Analysis*

The GPS logs between simulations and experiments were collected using a 4 waypoint configuration. Waypoints 1 and 2 have almost the same distance, while waypoint 3 is similar to waypoint 4. Each waypoint is tested in four trials. So a total of 16 trials. The characteristics of waypoints 1 and 2 are characteristics of long routes and not sharp turns. While routes 3 and 4 have shorter characteristics but with a greater number of bends and are sharper.The waypoint in the study can be seen in Fig. 3.

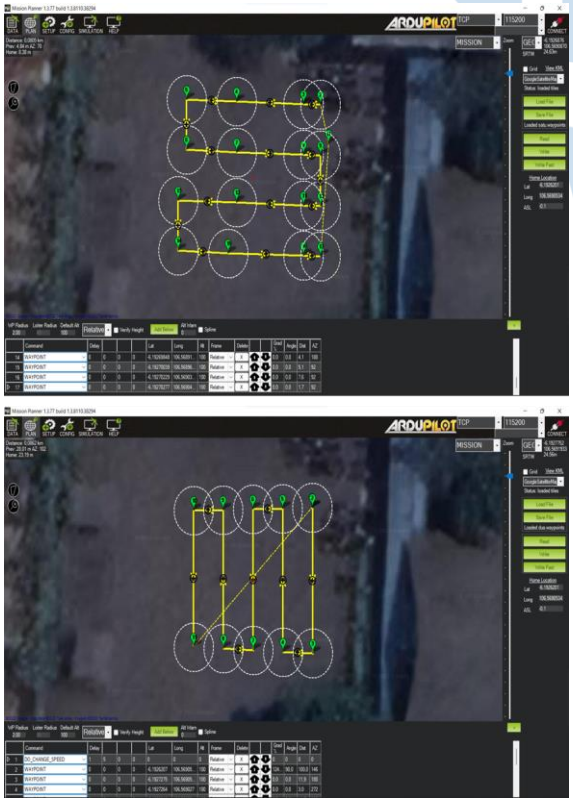

(a)

(b)

Fig. 3. (a) Rover Schematic, (b) Rover with Ardupilot controller

By referring to these waypoints, GPS points will be obtained, which are stored in the Ardupilot memory. Then, using the Mission Planner application, the GPS points are downloaded for analysis. The simulation used in this study is a SITL simulation on the Mission Planner application with the Rover vehicle selection mode. The GPS log from this simulation is analyzed to be compared with the experiment. Finding the difference between two GPS locations can be done with the use of the haversine formula. The difference between the two GPS points will be regarded as an error, and the accuracy value will be determined based on the data collected from the errors. The Haversine formula, which is based on the length of the straight line that connects the two points on the longitude and latitude axes, can be used to compute the distance between two points. The formula is based on the length of the straight line [17]:

$$\Delta lat = latitude2 - latitude1 \quad (1)$$

$$\Delta long = longitude2 - longitude1 \quad (2)$$

$$distance = 2.R.arcsin\left(\sqrt{sin^2\left(\frac{\Delta lat}{2}\right) + \cos(latitude2).\cos(latitude1).sin^2\left(\frac{\Delta long}{2}\right)}\right) \quad (3)$$

Where *R* is radius of earth in about 6371 km. After the experiment is complete, the difference between the simulation and experiment coordinates is determined by comparing them. The Root Mean Square Error *(RMSE)* is a commonly employed measure of the difference between the values predicted by the model

and the observed values from the environment being modeled. This *RMSE* parameter comes from the prediction model, and the square root of the squared mean error is used to describe the estimated variable *X* [18].

$$RMSE = \sqrt{\frac{\sum_{i=1}^{n}\left(X_{sim,i} - X_{exp,i}\right)^2}{n}} \quad (4)$$

Where, X_{sim} is value from simulation, and X_{exp} is value from experiment. Chen et al. analyzed the error of different GPS coordinates of experimental results and predictions using *RMSE* [19], in addition to Koo et al., who analyze GPS displacement using *RMSE* [20], so this study also uses the same method.

III. Result

A. Comparison of Mission Data

The data that has been obtained is then displayed in several types of data. The first result is the result of a comparison between routes (waypoints) compared to simulations and experiments. The data used to create the graph below consists of 100 coordinate points for each simulation and experiment, as well as four reference waypoints. The results of the comparison of missions, experiments, and simulations are as follows.

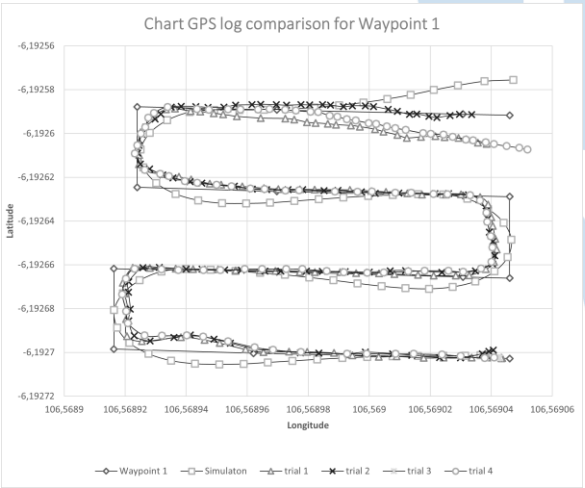

Fig. 4. GPS log comparison for Waypoint 1

Fig. 4 shows the route comparison between waypoint 1, as a reference, simulation, experiment 1, experiment 2, experiment 3, and experiment 4 with the number of coordinate points used of 100 data point coordinates, except for waypoint 1.

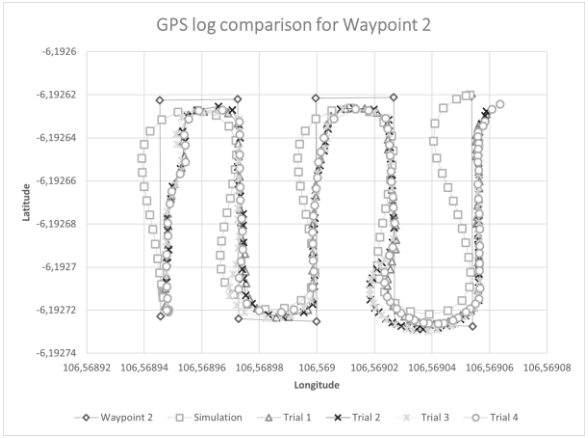

Fig. 5. Chart GPS log comparison for Waypoint 2

Fig. 5 shows the route comparison between waypoint 2, as a reference, simulation, experiment 1, experiment 2, experiment 3, and experiment 4 with the number of coordinate points used of 100 data point coordinates, except for waypoint 2.

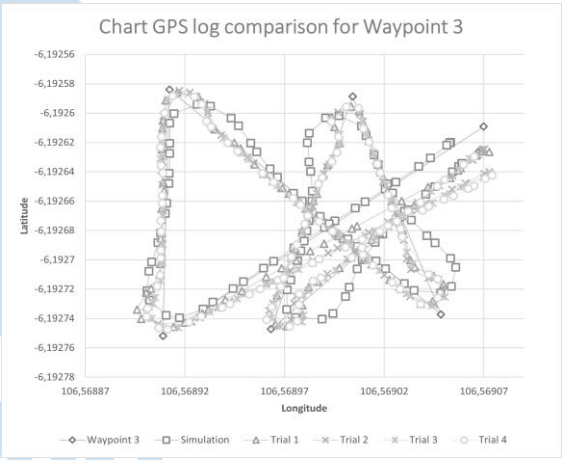

Fig. 6. Chart GPS log comparison for Waypoint 3

Fig. 6 shows the route comparison between waypoint 3, as a reference, simulation, experiment 1, experiment 2, experiment 3, and experiment 4 with the number of coordinate points used of 100 data point coordinates, except for waypoint 3.

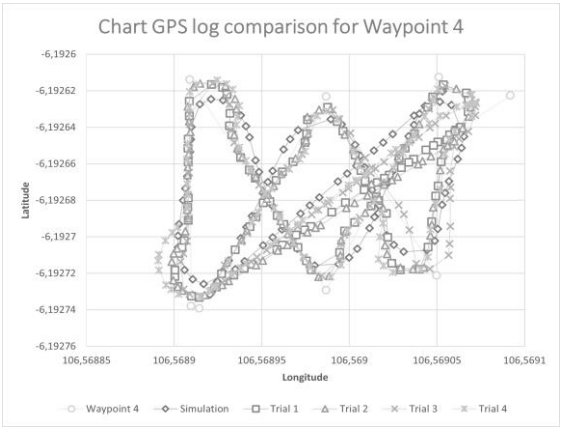

Fig. 7. Chart GPS log comparison for Waypoint 4

Fig. 7 shows the route comparison between waypoint 4, as a reference, simulation, experiment 1, experiment 2, experiment 3, and experiment 4 with the number of coordinate points used of 100 data point coordinates, except for waypoint 4.

B. Accuracy Analysis

Based on the data visualized in Fig 4, Fig 5, Fig 6, and Fig 7, accuracy analysis is carried out by calculating the difference in coordinates between the simulation and each experiment. The calculation of the distance between the coordinates using the haversine formula (1), (2), and (3). The results of the calculation of the average accuracy shown in Table I.

TABLE I. ACCURACY ANALYSIS RESULTS

No	Waypoint	Trial	Accuracy (%)
1	Waypoint 1	1st	92,54
		2nd	92,31
		3rd	92,47
		4th	91,87
2	Waypoint 2	1st	94,42
		2nd	94,28
		3rd	94,73
		4th	94,87
3	Waypoint 3	1st	97,78
		2nd	96,86
		3rd	97,00
		4th	97,58
4	Waypoint 4	1st	94,16
		2nd	94,79
		3rd	94,12
		4th	93,47
Average			94,58

Based on the data in Table I, it can be seen that the average accuracy of the robot navigation system based on a comparison of simulations and experiments can be seen to be 94.58%. The smallest experimental accuracy is in the waypoint 1 experiment, with the characteristics of a long route and relatively blunt bends. The highest experimental accuracy value is found in the waypoint 3 experiment, which has the characteristics of the shortest route even though it has the sharpest bend, but the accuracy level remains the highest.

C. GPS Data Analysis with RMSE

The formula used to determine the *RMSE* between experimental results and simulation results is as follows (4). Each research utilizes a sample size of 100. Table II shows the results of the *RMSE* analysis.

TABLE II. THE RESULT OF THE RMSE ANALYSIS OF THE COORDINATES

No	Waypoint	Trial	Accuracy (%)
1	Waypoint 1	1st	$7,63 \times 10^{-5}$
		2nd	$7,86 \times 10^{-5}$
		3rd	$7,74 \times 10^{-5}$
		4th	$8,08 \times 10^{-5}$
2	Waypoint 2	1st	$5,74 \times 10^{-5}$
		2nd	$5,88 \times 10^{-5}$
		3rd	$5,40 \times 10^{-5}$
		4th	$5,29 \times 10^{-5}$
3	Waypoint 3	1st	$2,40 \times 10^{-5}$
		2nd	$2,90 \times 10^{-5}$
		3rd	$2,84 \times 10^{-5}$
		4th	$2,50 \times 10^{-5}$
4	Waypoint 4	1st	$5,74 \times 10^{-5}$
		2nd	$5,19 \times 10^{-5}$
		3rd	$5,79 \times 10^{-5}$
		4th	$6,70 \times 10^{-5}$

According to Table II, the *RMSE* value for the waypoint 3 experiment is the one with the least amount of variance. The results of this investigation are the same as the analysis of accuracy shown in Table I.

IV. CONCLUSION

The accuracy of the robot navigation system, based on a comparison of simulations and experiments, can be seen to be 94.58%. The smallest experimental accuracy is in the waypoint 1 experiment, with the characteristics of a long route and relatively blunt bends, with an average accuracy of about 92,30% . The highest experimental accuracy value is found in the waypoint 3 experiment, with an average accuracy of about 97,31 %, which has the characteristics of the shortest route even though it has the sharpest bend, but the accuracy level remains the highest. Accordingly, the *RMSE* value is also the smallest in the waypoint 3 experiment and the largest in the waypoint 1 experiment. The long route may be the cause of the lack of accuracy in the rover's autonomous navigation. The turning angle problem in this case does not have an appreciable effect on the accuracy and performance of the rover's autonomous navigation.

ACKNOWLEDGEMENT

The authors are grateful to the Ministry of Education and Culture of Indonesia, Director of Polytechnic Gajah Tunggal, Head of Research and Community Service, Head of Electronic Engineering Study Program, and Head of Mechanical Engineering Study Program of Polytechnic Gajah Tunggal. Ministry of Education, Culture, Research and Technology of the Republic of Indonesia Grant.

REFERENCES

[1] M. N. Mikhaylov and I. A. Lositskii, “Control and navigation of forest robot,” 25th Saint Petersbg. Int. Conf. Integr. Navig. Syst. ICINS 2018 - Proc., pp. 1–2, 2018, doi: 10.23919/ICINS.2018.8405881.

[2] [K. A. Ghamry, M. A. Kamel, and Y. Zhang, "Cooperative forest monitoring and fire detection using a team of UAVs-UGVs," 2016 Int. Conf. Unmanned Aircr. Syst. ICUAS 2016, no. December 2017, pp. 1206–1211, 2016, doi: 10.1109/ICUAS.2016.7502585.

[3] L. Merino, F. Caballero, J. R. Martínez-De-Dios, I. Maza, and A. Ollero, "An unmanned aircraft system for automatic forest fire monitoring and measurement," J. Intell. Robot. Syst. Theory Appl., vol. 65, no. 1–4, pp. 533–548, 2012, doi: 10.1007/s10846-011-9560-x.

[4] J. Quenzel et al., "Autonomous Fire Fighting with a UAV-UGV Team at MBZIRC 2020," 2021 Int. Conf. Unmanned Aircr. Syst. ICUAS 2021, pp. 934–941, 2021, doi: 10.1109/ICUAS51884.2021.9476846.

[5] Z. Luo, X. Xiang, and Q. Zhang, Autopilot system of remotely operated vehicle based on ardupilot, vol. 11742 LNAI. Springer International Publishing, 2019.

[6] S. Oltean, "Mobile Robot Robot Platform Platform with with Arduino Arduino Uno and Raspberry Raspberry Pi for Autonomous Navigation," Procedia Manuf., vol. 32, pp. 572–577, 2019, doi: 10.1016/j.promfg.2019.02.254.

[7] A. Srisuphab, P. Silapachote, W. Tantratorn, P. Krakornkul, and P. Darote, "Insect Detection on an Unmanned Ground Rover," IEEE Reg. 10 Annu. Int. Conf. Proceedings/TENCON, vol. 2018-Octob, no. October, pp. 954–959, 2019, doi: 10.1109/TENCON.2018.8650312.

[8] M. Syazwan, A. Abdul, and A. Johar, "System Development of an Autonomous Lawnmower System Using Ardupilot Mission Planner," vol. 2, no. 2, pp. 533–538, 2021.

[9] S. Hassan, M. Alam, N. A. Siddiqui, A. A. Siddiqui, and M. T. Qadri, "Designing and control of autonomous Unmanned Ground Vehicle," in 2017 International Conference on Innovations in Electrical Engineering and Computational Technologies (ICIEECT), Apr. 2017, pp. 1–5, doi: 10.1109/ICIEECT.2017.7916547.

[10] Q. A. Nguyen, E. Grolleau, and H. K. Ngo, "Results and comparision between different control algorithms for a quadrotor using ArduPilot framework," Sci. Technol. Dev. J., vol. 18, no. 4, pp. 170–178, 2015, doi: 10.32508/stdj.v18i4.1003.

[11] A. F. Anto and T. Sukardiyono, "Prototype Autonomous Rover Pembersih Sampah Pantai menggunakan ArduPilot," Elinvo (Electronics, Informatics, Vocat. Educ., vol. 4, no. 2, pp. 202–209, 2019, doi: 10.21831/elinvo.v4i2.28793.

.

[12] D. F. Carlson and S. Rysgaard, "Adapting open-source drone autopilots for real-time iceberg observations," MethodsX, vol. 5, pp. 1059–1072, 2018, doi: 10.1016/j.mex.2018.09.003.

[13] C. Liu, O. McAree, and W.-H. Chen, "Path-following control for small fixed-wing unmanned aerial vehicles under wind disturbances," Int. J. Robust Nonlinear Control, vol. 18, no. December 2012, p. n/a-n/a, Dec. 2012, doi: 10.1002/rnc.2938.

[14] A. Janarthanan, H. W. Ho, L. Gopal, V. Shanmugam, and W. K. Wong, "An Unmanned Aerial Vehicle Framework Design for Autonomous Flight Path," 2019 7th Int. Conf. Smart Comput. Commun. ICSCC 2019, pp. 0–4, 2019, doi: 10.1109/ICSCC.2019.8843618.

[15] S. Jung and K. B. Ariyur, "Compensating UAV GPS data accuracy through use of relative positioning and GPS data of UGV," J. Mech. Sci. Technol., vol. 31, no. 9, pp. 4471–4480, 2017, doi: 10.1007/s12206-017-0847-0.

[16] S. Timpitak, P. Prempraneerach, M. Janthong, and E. Pengwang, "Small Unmanned Surface Vehicle In Autonomous Way-Point Experiment And Simulations For Straight Path Tracker," Suranaree J. Sci. Technol., vol. 28, no. 2, pp. 1–7, 2021.

[17] R. A. Azdy and F. Darnis, "Use of Haversine Formula in Finding Distance between Temporary Shelter and Waste End Processing Sites," J. Phys. Conf. Ser., vol. 1500, no. 1, 2020, doi: 10.1088/1742-6596/1500/1/012104.

[18] W. Widada, "Metode Penggabungan Beberapa Penerima Gps Untuk Roket Balistik (Method of Combining Multi-Gps Receivers To Improve Accuracy and Reliability of the Tracking System of Sounding Rocket)," J. Teknol. Dirgant., vol. 12, no. 1, pp. 1–10, 2013.

[19] B. Chen, H. Mei, Z. Li, Z. Wang, Y. Yu, and H. Yu, "Retrieving three-dimensional large surface displacements in coal mining areas by combining SAR pixel offset measurements with an improved mining subsidence model," *Remote Sens.*, vol. 13, no. 13, 2021, doi: 10.3390/rs13132541.

[20] G. Koo *et al.*, "Development of a high precision displacement measurement system by fusing a low cost RTK-GPS sensor and a force feedback accelerometer for infrastructure monitoring," *Sensors (Switzerland)*, vol. 17, no. 12, 2017, doi: 10.3390/s17122745.

AUTHOR GUIDELINES

1. Manuscript criteria

- The article has never been published or in the submission process on other publications.
- Submitted articles could be original research articles or technical notes.
- The similarity score from plagiarism checker software such as Turnitin is 20% maximum.
- For December 2021 publication onwards, Ultima Computing : Jurnal Sistem Komputer will be receiving and publishing manuscripts written in English only.

2. Manuscript format

- Article been type in Microsoft Word version 2007 or later.
- Article been typed with 1 line spacing on an A4 paper size (21 cm x 29,7 cm), top-left margin are 3 cm and bottom-right margin are 2 cm, and Times New Roman's font type.
- Article should be prepared according to the following author guidelines in this template. Article contain of minimum 3500 words.
- References contain of minimum 15 references (primary references) from reputable journals/conferences

3. Organization of submitted article

The organization of the submitted article consists of Title, Abstract, Index Terms, Introduction, Method, Result and Discussion, Conclusion, Appendix (if any), Acknowledgment (if any), and References.

- Title
  The maximum words count on the title is 12 words (including the subtitle if available)
- Abstract
  Abstract consists of 150-250 words. The abstract should contain logical argumentation of the research taken, problem-solving methodology, research results, and a brief conclusion.
- Index terms
  A list in alphabetical order in between 4 to 6 words or short phrases separated by a semicolon (;), excluding words used in the title and chosen carefully to reflect the precise content of the paper.
- Introduction
  Introduction commonly contains the background, purpose of the research, problem identification, research methodology, and state of the art conducted by the authors which describe implicitly.
- Method
  Include sufficient details for the work to be repeated. Where specific equipment and materials are named, the manufacturer's details (name, city and country) should be given so that readers can trace specifications by contacting the manufacturer. Where commercially available software has been used, details of the supplier should be given in brackets or the reference given in full in the reference list.
- Results and Discussion
  State the results of experimental or modeling work, drawing attention to important details in tables and figures, and discuss them intensively by comparing and/or citing other references.
- Conclusion
  Explicitly describes the research's results been taken. Future works or suggestion could be explained after it
- Appendix and acknowledgment, if available, could be placed after Conclusion.
- All citations in the article should be written on References consecutively based on its' appearance order in the article using Mendeley (recommendation). The typing format will be in the same format as the IEEE journals and transaction format.

4. Reviewing of Manuscripts

Every submitted paper is independently and blindly reviewed by at least two peer-reviewers. The decision for publication, amendment, or rejection is based upon their reports/recommendations. If two or more reviewers consider a manuscript unsuitable for publication in this journal, a statement explaining the basis for the decision will be sent to the authors within six months of the submission date.

5. Revision of Manuscripts

Manuscripts sent back to the authors for revision should be returned to the editor without delay (maximum of two weeks). Revised manuscripts can be sent to the editorial office through the same online system. Revised manuscripts returned later than one month will be considered as new submissions.

6. Editing References

- **Periodicals**
  J.K. Author, “Name of paper,” Abbrev. Title of Periodical, vol. x, no. x, pp. xxx-xxx, Sept. 2013.

- **Book**
  J.K. Author, “Title of chapter in the book,” in Title of His Published Book, xth ed. City of Publisher, Country or Nation: Abbrev. Of Publisher, year, ch. x, sec. x, pp xxx-xxx.

- **Report**
  J.K. Author, “Title of report,” Abbrev. Name of Co., City of Co., Abbrev. State, Rep. xxx, year.

- **Handbook**
  Name of Manual/ Handbook, x ed., Abbrev. Name of Co., City of Co., Abbrev. State, year, pp. xxx-xxx.

- **Published Conference Proceedings**
  J.K. Author, “Title of paper,” in Unabbreviated Name of Conf., City of Conf., Abbrev. State (if given), year, pp. xxx-xxx.

- **Papers Presented at Conferences**
  J.K. Author, “Title of paper,” presented at the Unabbrev. Name of Conf., City of Conf., Abbrev. State, year.

- **Patents**
  J.K. Author, “Title of patent,” US. Patent xxxxxxx, Abbrev. 01 January 2014.

- **Theses and Dissertations**
  J.K. Author, “Title of thesis,” M.Sc. thesis, Abbrev. Dept., Abbrev. Univ., City of Univ., Abbrev. State, year. J.K. Author, “Title of dissertation,” Ph.D. dissertation, Abbrev. Dept., Abbrev. Univ., City of Univ., Abbrev. State, year.

- **Unpublished**
  J.K. Author, “Title of paper,” unpublished. J.K. Author, “Title of paper,” Abbrev. Title of Journal, in press.

- **On-line Sources**
  J.K. Author. (year, month day). Title (edition) [Type of medium]. Available: http:// www.(URL) J.K. Author. (year, month). Title. Journal [Type of medium]. volume(issue), pp. if given. Available: http://www.(URL) Note: type of medium could be online media, CD-ROM, USB, etc.

7. Editorial Adress

Jl. Scientia Boulevard, Gading Serpong
Tangerang, Banten, 15811
Email: **ultimacomputing@umn.ac.id**

Paper Title

Subtitle (if needed)

Author 1 Name[1], Author 2 Name[2], Author 3 Name[2]
[1] Line 1 (of affiliation): dept. name of organization, organization name, City, Country
Line 2: e-mail address if desired
[2] Line 1 (of affiliation): dept. name of organization, organization name, City, Country
Line 2: e-mail address if desired

Accepted on mmmmm dd, yyyy
Approved on mmmmm dd, yyyy

***Abstract*—This electronic document is a "live" template which you can use on preparing your Ultima Computing paper. Use this document as a template if you are using Microsoft Word 2007 or later. Otherwise, use this document as an instruction set. Do not use symbol, special characters, or Math in Paper Title and Abstract. Do not cite references in the abstract.**

***Index Terms*—enter key words or phrases in alphabetical order, separated by semicolon (;)**

I. INTRODUCTION

This template, modified in MS Word 2007 and saved as a Word 97-2003 document, provides authors with most of the formatting specifications needed for preparing electronic versions of their papers. Margins, column widths, line spacing, and type styles are built-in here. The authors must make sure that their paper has fulfilled all the formatting stated here.

Introduction commonly contains the background, purpose of the research, problem identification, and research methodology conducted by the authors which been describe implicitly. Except for Introduction and Conclusion, other chapter's title must be explicitly represent the content of the chapter.

II. EASE OF USE

A. Selecting a Template

First, confirm that you have the correct template for your paper size. This template is for Ultima Computing. It has been tailored for output on the A4 paper size.

B. Maintaining the Integrity of the Specifications

The template is used to format your paper and style the text. All margins, column widths, line spaces, and text fonts are prescribed; please do not alter them.

III. PREPARE YOUR PAPER BEFORE STYLING

Before you begin to format your paper, first write and save the content as a separate text file. Keep your text and graphic files separate until after the text has been formatted and styled. Do not add any kind of pagination anywhere in the paper. Please take note of the following items when proofreading spelling and grammar.

A. Abbreviations and Acronyms

Define abbreviations and acronyms the first time they are used in the text, even after they have been defined in the abstract. Abbreviations such as IEEE, SI, MKS, CGS, sc, dc, and rms do not have to be defined. Abbreviations that incorporate periods should not have spaces: write "C.N.R.S.," not "C. N. R. S." Do not use abbreviations in the title or heads unless they are unavoidable.

B. Units

- Use either SI (MKS) or CGS as primary units (SI units are encouraged).
- Do not mix complete spellings and abbreviations of units: "Wb/m2" or "webers per square meter," not "webers/m2." Spell units when they appear in text: "...a few henries," not "...a few H."
- Use a zero before decimal points: "0.25," not ".25."

C. Equations

The equations are an exception to the prescribed specifications of this template. You will need to determine whether or not your equation should be typed using either the Times New Roman or the Symbol font (please no other font). To create multileveled equations, it may be necessary to treat the equation as a graphic and insert it into the text after your paper is styled.

Number the equations consecutively. Equation numbers, within parentheses, are to position flush right, as in (1), using a right tab stop.

$$\int_0^{r_2} F(r,\phi)\, dr\, d\phi = [\sigma r_2 / (2\mu_0)] \qquad (1)$$

Note that the equation is centered using a center tab stop. Be sure that the symbols in your equation have been defined before or immediately following the

equation. Use "(1)," not "Eq. (1)" or "equation (1)," except at the beginning of a sentence: "Equation (1) is ..."

D. Some Common Mistakes

- The word "data" is plural, not singular.
- The subscript for the permeability of vacuum μ_0, and other common scientific constants, is zero with subscript formatting, not a lowercase letter "o."
- In American English, commas, semi-/colons, periods, question and exclamation marks are located within quotation marks only when a complete thought or name is cited, such as a title or full quotation. When quotation marks are used, instead of a bold or italic typeface, to highlight a word or phrase, punctuation should appear outside of the quotation marks. A parenthetical phrase or statement at the end of a sentence is punctuated outside of the closing parenthesis (like this). (A parenthetical sentence is punctuated within the parentheses.)
- A graph within a graph is an "inset," not an "insert." The word alternatively is preferred to the word "alternately" (unless you really mean something that alternates).
- Do not use the word "essentially" to mean "approximately" or "effectively."
- In your paper title, if the words "that uses" can accurately replace the word using, capitalize the "u"; if not, keep using lower-cased.
- Be aware of the different meanings of the homophones "affect" and "effect," "complement" and "compliment," "discreet" and "discrete," "principal" and "principle."
- Do not confuse "imply" and "infer."
- The prefix "non" is not a word; it should be joined to the word it modifies, usually without a hyphen.
- There is no period after the "et" in the Latin abbreviation "et al."
- The abbreviation "i.e." means "that is," and the abbreviation "e.g." means "for example."

IV. Using the Template

After the text edit has been completed, the paper is ready for the template. Duplicate the template file by using the Save As command, and use the naming convention as below

ULTIMATICS_firstAuthorName_paperTitle.

In this newly created file, highlight all of the contents and import your prepared text file. You are now ready to style your paper. Please take note on the following items.

A. Authors and Affiliations

The template is designed so that author affiliations are not repeated each time for multiple authors of the same affiliation. Please keep your affiliations as succinct as possible (for example, do not differentiate among departments of the same organization).

B. Identify the Headings

Headings, or heads, are organizational devices that guide the reader through your paper. There are two types: component heads and text heads.

Component heads identify the different components of your paper and are not topically subordinate to each other. Examples include ACKNOWLEDGMENTS and REFERENCES, and for these, the correct style to use is "Heading 5."

Text heads organize the topics on a relational, hierarchical basis. For example, the paper title is the primary text head because all subsequent material relates and elaborates on this one topic. If there are two or more sub-topics, the next level head (uppercase Roman numerals) should be used and, conversely, if there are not at least two sub-topics, then no subheads should be introduced. Styles, named "Heading 1," "Heading 2," "Heading 3," and "Heading 4", are prescribed.

C. Figures and Tables

Place figures and tables at the top and bottom of columns. Avoid placing them in the middle of columns. Large figures and tables may span across both columns. Figure captions should be below the figures; table heads should appear above the tables. Insert figures and tables after they are cited in the text. Use the abbreviation "Fig. 1," even at the beginning of a sentence.

TABLE I. TABLE STYLES

Table Head	**Table Column Head**		
	Table column subhead	***Subhead***	***Subhead***
copy	More table copy		

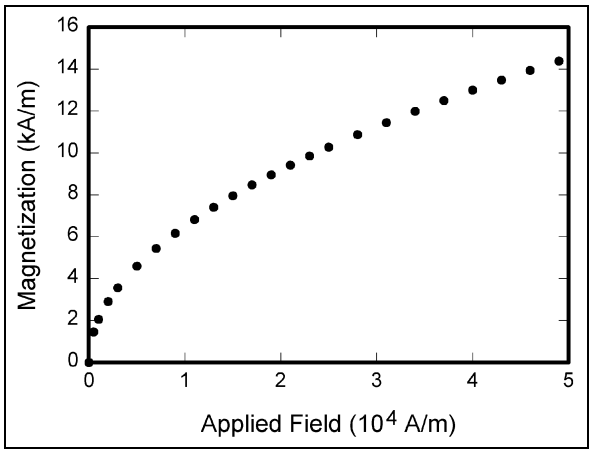

Fig. 1. Example of a figure caption

V. Conclusion

A conclusion section is not required. Although a conclusion may review the main points of the paper, do not replicate the abstract as the conclusion. A conclusion might elaborate on the importance of the work or suggest applications and extensions.

Appendix

Appendixes, if needed, appear before the acknowledgment.

ACKNOWLEDGMENT

The preferred spelling of the word "acknowledgment" in American English is without an "e" after the "g." Use the singular heading even if you have many acknowledgments. Avoid expressions such as "One of us (S.B.A.) would like to thank ... ." Instead, write "F. A. Author thanks ... ." You could also state the sponsor and financial support acknowledgments here.

References

The template will number citations consecutively within brackets [1]. The sentence punctuation follows the bracket [2]. Refer simply to the reference number, as in [3]—do not use "Ref. [3]" or "reference [3]" except at the beginning of a sentence: "Reference [3] was the first ..."

Number footnotes separately in superscripts. Place the actual footnote at the bottom of the column in which it was cited. Do not put footnotes in the reference list. Use letters for table footnotes.

Unless there are six authors or more give all authors' names; do not use "et al.". Papers that have not been published, even if they have been submitted for publication, should be cited as "unpublished" [4]. Papers that have been accepted for publication should be cited as "in press" [5]. Capitalize only the first word in a paper title, except for proper nouns and element symbols.

For papers published in translation journals, please give the English citation first, followed by the original foreign-language citation [6].

[1] G. Eason, B. Noble, and I.N. Sneddon, "On certain integrals of Lipschitz-Hankel type involving products of Bessel functions," Phil. Trans. Roy. Soc. London, vol. A247, pp. 529-551, April 1955. (*references*)

[2] J. Clerk Maxwell, A Treatise on Electricity and Magnetism, 3rd ed., vol. 2. Oxford: Clarendon, 1892, pp.68-73.

[3] I.S. Jacobs and C.P. Bean, "Fine particles, thin films and exchange anisotropy," in Magnetism, vol. III, G.T. Rado and H. Suhl, Eds. New York: Academic, 1963, pp. 271-350.

[4] K. Elissa, "Title of paper if known," unpublished.

[5] R. Nicole, "Title of paper with only first word capitalized," J. Name Stand. Abbrev., in press.

[6] Y. Yorozu, M. Hirano, K. Oka, and Y. Tagawa, "Electron spectroscopy studies on magneto-optical media and plastic substrate interface," IEEE Transl. J. Magn. Japan, vol. 2, pp. 740-741, August 1987 [Digests 9th Annual Conf. Magnetics Japan, p. 301, 1982].

[7] M. Young, The Technical Writer's Handbook. Mill Valley, CA: University Science, 1989.

UMN

UNIVERSITAS
MULTIMEDIA
NUSANTARA

ISSN 2355-3286

UMN
UNIVERSITAS
MULTIMEDIA
NUSANTARA

PRESS

Universitas Multimedia Nusantara
Scientia Garden Jl. Boulevard Gading Serpong, Tangerang
Telp. (021) 5422 0808 | Fax. (021) 5422 0800